

# **ENVIRONMENTAL DURABILITY OF CFRP STRAND SHEETS STRENGTHENED STEEL PLATE DOUBLE STRAP JOINTS**

---

A Thesis

Presented to

the faculty of the School of Engineering and Applied Science

University of Virginia

---

in partial fulfillment  
of the requirements for the degree

Master of Science

by

Yuhui Lyu

May 2018

# APPROVAL SHEET

This Thesis  
is submitted in partial fulfillment of the requirements  
for the degree of  
Master of Science

Author Signature: Yuhui Lyu

This Thesis has been read and approved by the examining committee:

Advisor: Osman E. Ozbulut

Committee Member: Jose P. Gomez III

Committee Member: Devin K. Harris

Committee Member: \_\_\_\_\_

Committee Member: \_\_\_\_\_

Committee Member: \_\_\_\_\_

Accepted for the School of Engineering and Applied Science:



Craig H. Benson, School of Engineering and Applied Science

May 2018

## ABSTRACT

Steel bridges exposed to aggressive environments such as coastal conditions can experience damage due to various deterioration mechanisms. One of the most important threats during lifetime of a steel bridge structure is the corrosion. The deterioration of steel bridges due to corrosion decreases the lifespan and reliability of the system and leads to reduction in serviceability and aesthetics of the structure. In addition, with the incorporation of new legal load models into load rating process, many existing short to medium span steel bridges are now rated as structurally deficient in live load capacity. Therefore, many state transportation agencies need to strengthen steel bridges due to increases in live loads or loss of capacity as a result of environmental deterioration. Fiber reinforced polymers (FRPs) have been widely considered to restore stiffness and strength of concrete bridges due to their favorable properties such as high corrosion resistance, lightweight and high tensile strength. However, their applications to steel bridges have been limited. Several studies showed that the use of high modulus carbon FRP (CFRP) laminates or sheets can significantly increase both the ultimate flexural capacity and the stiffness of steel beams, but the premature debonding failure was commonly observed. More recently, a new form of CFRPs that consists of small-diameter strands have been shown to possess excellent bond characteristics and great potential for flexural and shear strengthening of steel girder bridges through laboratory investigations. However, the environmental durability of steel members strengthened with CFRP strand sheets has not been studied yet.

This study investigates the durability of CFRP strand sheet-steel plate double strap joints in accelerated corrosion conditions. The CFRP-steel double strap joint specimens with different bond lengths were fabricated. The specimens were subjected to different levels of accelerated corrosion conditions using an electrochemical method for three exposure durations corresponding to 5%, 10%, and 15% mass losses based on the Faraday's law. Then, tensile testing of double strap joints was conducted on an MTS frame up to failure. Results were analyzed in terms of bond strength, effective bond length and joint stiffness considering different exposure durations. Failure modes of specimens with different bond lengths and exposed to different levels of corrosion were also discussed.

## **DEDICATION**

To my parents, Xiuzhen Huang and Deyong Lyu, and my boyfriend, Zhuozhao Li, for their endless support and company.

## **ACKNOWLEDGEMENTS**

I would like to thank the faculty and staff of the Department of Civil Engineering of University of Virginia and the Virginia Transportation Research Council (VTRC). In particular, I would like to express my sincere gratitude to my advisor, Dr. Osman Ozbulut, for his guidance and support throughout my thesis work. I would also like to thank Dr. Devin Harris and Dr. Gomez for serving on my thesis defense committee.

I am grateful to Mr. Keegan Gumbs, Structures Lab Manager, for his support on specimen fabrication. I would also like to thank Mr. Arthur W. Ordell, Engineering Technician at VTRC, for his help and guidance during experimental testing. I would like to express my deepest appreciation to my laboratory mates, Mr. Muhammad M. Sherif and Mr. Sherif Daghash, for their support on my research. Finally, I would like to thank to my family for their ceaseless support.

## NOMENCLATURE

CFRP	Carbon Fiber Reinforcement polymer
HM	High Modulus
T <sub>g</sub>	Glass Transition Temperature
UV	Ultraviolet Radiation
CR	Corrosion Rate
MR	Mass Loss Rate
g/m <sup>2</sup> d	Gram Per Unit Area Per Day
N	Negative
P	Positive

# TABLE OF CONTENTS

ABSTRACT.....	1
DEDICATION.....	2
ACKNOWLEDGEMENTS.....	3
NOMENCLATURE.....	4
TABLE OF CONTENTS.....	5
LIST OF TABLES.....	8
LIST OF FIGURES.....	9
1. INTRODUCTION.....	11
1.1 Motivation.....	11
1.2 Research Objectives.....	13
1.3 Organization of Thesis.....	13
2. LITERATURE REVIEW.....	15
2.1 CFRP-Steel Double Strap Joints.....	15
2.1.1 Overview.....	15
2.1.2 Failure modes.....	15
2.1.3 Effect of surface preparation.....	16
2.1.4 Effect of primer.....	17
2.2 Environmental Durability of CFRP-Steel Double Strap Joints.....	17
2.3 Strengthening Steel Members Using CFRP Strand Sheets.....	22
2.4 Galvanic Corrosion.....	22
2.4.1 Theory.....	22
2.4.2 Faraday’s laws of electrolysis.....	24
3. EXPERIMENTAL DESIGN AND TESTING.....	26

3.1	Tensile Characterization of Materials .....	26
3.1.1	Adhesive .....	26
3.1.2	Primer.....	27
3.1.3	Single strand of CFRP .....	28
3.1.4	CFRP strand sheets .....	29
3.2	Fabrication of CFRP-Steel Double Strap Joint Specimens .....	30
3.2.1	Preparation of steel plates .....	32
3.2.2	Application of primer on the steel surface.....	33
3.2.3	Bonding CFRP sheets .....	33
3.2.4	Curing condition .....	37
3.3	Test Matrix .....	37
3.4	Accelerated Corrosion Environment.....	38
3.5	Test Set-up.....	40
4.	EXPERIMENTAL RESULTS.....	41
4.1	Mechanical Characteristics of Individual Components .....	41
4.1.1	Tensile response of adhesive .....	41
4.1.2	Tensile response of primer.....	42
4.1.3	Tensile response of individual CFRP strand.....	42
4.1.4	Tensile response of CFRP strand sheets .....	43
4.1.5	Summary of Tensile Tests .....	44
4.2	Specimen Characteristics After Accelerated Corrosion Exposure.....	45
4.2.1	Characterization of rusts and rust formation.....	45
4.2.2	Corrosion rate and mass loss rate.....	46
4.3	Tensile Test Results on CFRP-Steel Joints .....	49
4.3.1	Load-displacement curves .....	49

4.3.2	Effect of corrosion on joint stiffness.....	52
4.3.3	Effect of corrosion on joint effective bond length.....	54
4.3.4	Effect of corrosion on joint strength .....	56
4.3.5	Effect of corrosion on failure modes .....	59
5.	CONCLUSIONS AND RECOMMENDATIONS .....	61
	REFERENCES .....	63

## LIST OF TABLES

<b>Table 1.</b> Test matrix .....	37
<b>Table 2</b> Material properties of steel, CFRP strand, epoxy and primer .....	44
<b>Table 3.</b> Variation of physical properties with time .....	47
<b>Table 4</b> Summary of test results .....	55

## LIST OF FIGURES

Figure 1. Small-diameter CFRP strand sheet.....	12
Figure 2. Failure modes of double strap joints [30].....	16
Figure 3. Anodic and cathodic processes in a corrosion cell [54] .....	24
Figure 4. Adhesive tensile test samples: (a) in molds, (b) after curing .....	27
Figure 5. Test set-up for adhesive.....	27
Figure 6. Primer tensile test samples: (a) in molds, (b) after curing.....	28
Figure 7. Single CFRP strand tensile test samples: (a) in molds, (b) after curing.....	29
Figure 8. CFRP strand sheets (a) with aluminum tabs, (b) with CFRP woven sheet tabs	30
Figure 9. Schematic diagram of CFRP-steel double strap joint.....	31
Figure 10. Section view of CFRP-steel double strap joint.....	31
Figure 11. Sketches of (a) top and (b) mold molds used in fabrication of double strap joints	32
.....	
Figure 12. The contrast of steel surface before and after cleaning .....	33
Figure 13. Preparation of materials(a) carbon fiber strand sheets, (b) epoxy.....	34
Figure 14. Placing CFRP sheet to top and bottom mold.....	35
Figure 15. Placing steel plates on surface of epoxy .....	35
Figure 16. Connecting the top and bottom mold .....	36
Figure 17. Placing the mold into the clamping assembly .....	36
Figure 18. Applying pressure to molds by clamping.....	36
Figure 19. Typical layout of accelerated corrosion series circuit [60] .....	39
Figure 20. Schematic view of accelerated corrosion series circuit.....	39
Figure 21. Test set-up .....	40
Figure 22. Tensile stress-stain behavior of the epoxy.....	41
Figure 23. Tensile stress-stain behavior of the primer.....	42
Figure 24. Stress and strain curve for single CFRP strand .....	43
Figure 25. Stress and strain curve for CFRP strand sheets.....	44
Figure 26. Color transformation for BL75-B.....	45
Figure 27. Corrosion damage of edges of BL75-B.....	46
Figure 28. Variation of corrosion rate with exposure duration.....	48

Figure 29. Variation of mass loss rate with exposure duration.....	48
Figure 30. Load-displacement curve for specimens BL75-CS, BL125-CS and BL 175-CS .....	50
Figure 31. Load-displacement curve for specimens BL75-A, BL75-B and BL75-C.....	50
Figure 32. Load-displacement curve for specimens BL125-A, BL125-B and BL125-C	51
Figure 33. Load-displacement curve for specimens BL175-A, BL175-B and BL 175-C	51
Figure 34. Stiffness-exposure time relationship for specimen BL75 .....	52
Figure 35. Stiffness-exposure time relationship for specimen BL125 .....	53
Figure 36. Stiffness-exposure time relationship for specimen BL175 .....	53
Figure 37. Stiffness-exposure time relationship for specimens BL75, BL125 and BL175 .....	54
Figure 38. Ultimate load capacity versus bond length.....	56
Figure 39. Strength-exposure time relationship for specimen BL75.....	57
Figure 40. Strength-exposure time relationship for specimen BL125.....	57
Figure 41. Strength-exposure time relationship for specimen BL175.....	58
Figure 42. Strength-exposure time relationship for specimens BL75, BL125 and BL175 .....	58
Figure 43. CFRP rupture at the gap .....	60
Figure 44. Debonding failure.....	60
Figure 45. Debonding of epoxy from primer.....	60

# 1. INTRODUCTION

## 1.1 Motivation

Over their service life, steel bridge structures need to be strengthened due to different factors [1]. Structural steel corrodes rapidly which on a bridge may lead to major retrofit or even sudden collapse [2-3]. Many steel bridge girders experience fatigue cracks after being subjected to cyclic tensile loads due to traffic after years in service [4]. In addition, new vehicles that play an important role in trucking industry were developed in recent years, as well as newer emergency response vehicles can have significant impact on highway infrastructure [5]. These vehicles can produce load effects, such as bending moment and shear, on some bridge spans that are substantially larger than those from standard legal-loads requiring additional consideration in the load rating process, even causing some structures to become deficient [6-7]. Replacement of all aging and structurally deficient bridges would require significant resources and time; however, strengthening provides a more economical and sustainable alternative to extend the intended lifespans of steel bridges.

Traditional strengthening methods to strengthen steel bridges usually consist of welding or bolting steel plates to the structure. But these traditional methods suffer from inherent drawbacks such as further corrosion threat. In addition, attaching steel plates to the structure may add extra weights, which makes some other steel members carry more loads. During welding or bolting, residual stress might be introduced to the structure, leading to the reduction in the fatigue strength. Moreover, traditional methods for strengthening steel bridges require heavy equipment for the transportation and installation of the materials and are labor-intensive, which increase maintenance costs [8-10].

Recently, the use of fiber reinforced polymer (FRP) materials for the repair and strengthening of steel structures has gained attraction due to the remarkable mechanical properties of FRP such as high specific strength and stiffness and corrosion resistance. In addition, high labor and cost demands for strengthening can be avoided when the FRPs are used for strengthening applications due to their light weight [11-12]. Glass fiber-reinforced polymer (GFRP) composites and carbon fiber-reinforced polymer (CFRP) composites have been most commonly used FRP materials in civil engineering. However, due to the low-tensile modulus of GFRP, it is less desirable for retrofitting steel structures [13-14]. On the other hand, CFRP has excellent properties

that are suitable for strengthening steel structures such as high tensile strength and elastic modulus, good corrosion resistance and fatigue properties. Therefore, CFRPs have been explored for use in strengthening and repair of deteriorated steel structures.

Initial studies found that strengthening steel girders with CFRPs significantly increases the flexural strength but offers a very limited increase in stiffness of girders [15-18]. A very large amount of FRP material might be required to achieve satisfactory increases in the elastic stiffness due to relatively low modulus of elasticity and possibly due to presence of a shear-lag effect between the steel surface and the FRP [19]. Several researchers have studied the development and use of high modulus CFRP laminates or sheets to increase both the ultimate flexural capacity and the stiffness of steel beams [19-21]. Satisfactory performance was obtained and the guidelines on the use of externally bonded high modulus CFRP materials for flexural strengthening of steel girders were proposed [22]. However, several researchers reported premature debonding failure of the CFRP laminates [23-24]. In addition, to increase the total load carrying capacity of a bridge girder, not only flexural capacity but also the shear capacity of the steel girders should be increased. The use of CFRPs in shear strengthening of steel girders has been limited mainly due to debonding failure observed in compressive regions [25-26].

More recently, a new form of CFRPs that consists of small-diameter strands has been shown to possess excellent bond characteristics and great potential for flexural and shear strengthening of steel girder bridges through laboratory investigations [27-28]. These CFRP strands, provided in a sheet configuration, have a diameter of approximately 1 mm (1/25 inch) and are stitched together leaving a gap between the strands as shown in Figure 1. The gap between the strands can be filled with adhesive material, providing a contact with entire perimeter of the material compared to bonding of conventional CFRP strips through only one surface. It was shown that the small diameter CFRP strands eliminates any possible debonding up to failure in tension and compression [28-29].



**Figure 1.** Small-diameter CFRP strand sheet

Although the effectiveness of small-diameter CFRP strand sheets in strengthening steel members was shown, long-term environmental durability of CFRP strand sheet-steel strengthened joints have not been studied yet. Therefore, this thesis mainly focuses on the bond behavior and environmental durability of CFRP-steel double strap joints.

## **1.2 Research Objectives**

Since steel structures are typically exposed to a wide range of environmental conditions, the environmental durability of a strengthening system is essential to ensure satisfactory long-term performance of the system. This thesis investigates the durability of CFRP strand sheet strengthened steel plate double strap joints in accelerated corrosion conditions. First, CFRP-steel double strap joint specimens were fabricated using different effective bond lengths. The specimens were subjected to different levels of accelerated corrosion conditions using an electrochemical method. In particular, three exposure durations corresponding to 5%, 10%, and 15% mass losses were considered. Double strap joints were tested under tensile loads on an MTS frame up to failure. Bond strength and stiffness of double strap joints were computed and, the relationship between bond strength and effective bond length of the double strap joints, defined as the maximum bond length beyond which no significant increase in load carrying capacity occur was studied. Failure modes of specimens with different bond lengths and exposed to different levels of corrosion were also discussed.

## **1.3 Organization of Thesis**

This thesis is organized into the following sections:

Chapter 1 describes the motivation for this research and gives a brief introduction of this research topic.

Chapter 2 presents a literature review related to strengthening steel structures with CFRP materials. More emphasis is placed on the research related to the characteristics of bonded joints under environmental conditions.

Chapter 3 explains the materials and equipment used in this research and discusses the experimental tests conducted in this study. The specimen fabrication process and material properties are also included in this chapter.

Chapter 4 discusses the experimental test results and provides a discussion on the effects of corrosion on the failure modes, effective bond length and ultimate load of double strap joints.

Chapter 5 summarizes the findings of the current study and provides concluding remarks and recommendations for potential further research.

## 2. LITERATURE REVIEW

In this section, a general description of CFRP-steel double strap joints along with a discussion on the effect of different parameters on the bond behavior of such joints is first provided. Then, previous studies on the environmentally durability characteristics of CFRP-steel double strap joints is reviewed. Finally, a brief overview on galvanic corrosion is presented.

### 2.1 CFRP-Steel Double Strap Joints

#### 2.1.1 Overview

In order to study bond behavior between FRP and steel members, shear joint tests such as single or double lap joint tests and double strap joint tests are usually conducted. In a lap joint test, the tensile loads are directly applied to the FRP component. In a single-lap joint tests, the FRP material is bonded to one of the steel surfaces and the loads are applied to the FRP. This causes eccentricities to be developed and bending of FRP layer. Double-lap joints eliminate this problem, but gripping FRP components is a challenge in that test configuration. Therefore, double strap joints where the load is directly applied on the steel plate have commonly been used in the literature. One of the concern in this test configuration is the uncertainty of debonding location. However, this can be overcome by using unequal bond lengths.

#### 2.1.2 Failure modes

Six types of failure could be observed in CFRP-steel joints under various conditions including [30]:

- CFRP rupture,
- steel plate yielding,
- CFRP delamination,
- failure in the adhesive layer (cohesive failure),
- debonding between the CFRP and the adhesive layer or
- debonding between the steel plates and the adhesive layer or the primer (adhesive failure).

Figure 2 shows a schematic view of these failure mechanisms for double strap joints. The influence of various factors on failure mechanism of these joints is discussed in the following sections.

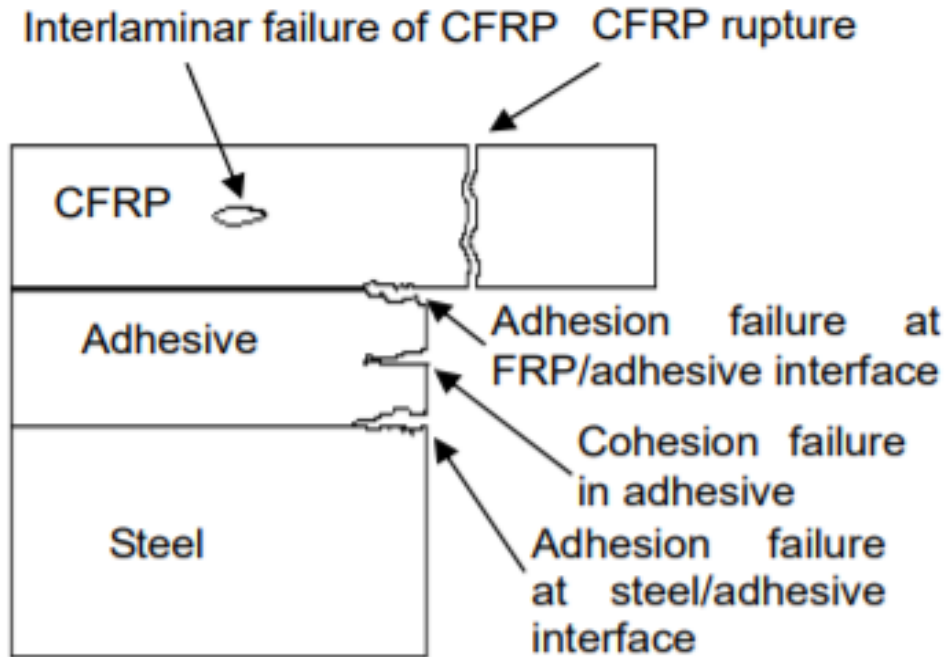


**Figure 2.** Failure modes of double strap joints [30]

### **2.1.3 Effect of surface preparation**

Surface preparation prior to bonding is of great importance in forming a strong bond because in previous studies failure was mainly observed at the steel/adhesive or steel/primer interface.

Fawzia et al. [31] recommended that steel plates should be sandblasted to remove all rust and paint and then the cross-sectional surfaces need to be cleaned with acetone before application of adhesive. Al-Zubaidy et al. [32] also noted that surface preparation has a significant influence on the bond between steel plate and CFRP. In their recommended surface preparation method, acetone is first used to remove any grease or paint. Then, sandblasting is used to remove any weak layers and rust. Finally, acetone is used again to remove abrasive dust on the sandblasted surface.

Liu et al. [33] explored the effect of surface preparation techniques on the bond behavior of CFRP-steel joints. The steel surface was treated by sandblasting or grinded by an angle grinder. Based on the results of experimental testing, they suggested that sand-blasting is more suitable than angle-grinding in steel surface preparation.

Batuwitage et al. [34] studied the failure modes and tensile capacity of CFRP/steel joints by using different surface preparation methods, including sandblasting, grit blasting and mechanically grinding. The results showed that sandblasting was the most efficient method to prepare the surface of steel plate when taking the load-carrying capacity and economic factors into consideration. The performance of the CFRP-steel interface cleaned by grit blasting was only slightly better than those of prepared by sandblasting. It was also found that mechanical grinding could not be used as a surface preparation method to create a strong bond.

#### **2.1.4 Effect of primer**

The goal of using primer in CFRP-steel joints is to protect the steel surface from galvanic corrosion by preventing the direct contact of CFRP materials with the steel substrate. Moreover, it can be used to smooth the rough steel surface to improve the bond behavior between steel substrate and adhesive.

Taylor et al. [35] investigated the bond behavior, bond strength and failure modes of double strap joints with and without a primer layer. The results showed that failure of joints without primer was observed in the interface between steel and CFRP. For the joints with primer, failure occurred in the interface between the primer and adhesive. The bond strength of joints without primer was about 15-42% higher than that of joints with primer.

Jiao et al. [27] studied the fatigue life of double strap joints bonded with or without the primer. After testing, the results showed that the primer caused a linear reduction in fatigue life due to the lower Yong's modulus of the primer resin.

Linghoff et al. [36] studied the behavior of beams strengthened with CFRP laminates. Primer were coated on the lower flange of the strengthened beams. After testing the beams, debonding between the primer and the steel substrate was found. This indicated that the adhesion between the primer and the steel substrate was poor and care needs to be given to the preparation of this layer.

## **2.2 Environmental Durability of CFRP-Steel Double Strap Joints**

Recent studies have shown that the use of CFRP can be an effective method for strengthening of steel structures. However, the bond behavior of steel structures strengthened with CFRP under various environmental conditions needs to be well-understood before field application

of this strengthening technique. Therefore, various studies have been conducted to assess environmental durability of CFRP-steel joints.

Al-Shawaf et al. [37] studied the short-term effect of subzero temperature on the bond characteristics between CFRP and steel plates. Tensile tests were conducted on the CFRP-steel double-strap joints subjected to 20°C, 0°C, -20°C, and -40°C environmental exposures. The results indicated that the debonding failure occurred at the adhesive/steel interface was the dominant failure mode after the joint specimens exposed to the short-term thermal exposure. It was shown that the sub-zero temperature did not have significant effect on the bond strength.

Heshmati et al. [38] investigated the durability of CFRP-steel joints under cyclic wet-dry and freeze-thaw conditions. The effects of cyclic wet-dry, freeze-thaw and combined wet and freeze-thaw conditions on the mechanical behavior of bonded CFRP-steel joints were studied. The results revealed that cohesive failure mode was the dominant failure mode of joint specimens under distilled water wet-dry condition. For specimens under salt-water conditions, the failure mode turned out to be interlaminar CFRP failure. The joint strength of specimens under both distilled water and salt water was decreased. However, freeze-thaw cycles had no negative effects on the strength of joints.

Nguyen et al. [39] examined the mechanical performance of CFRP-steel joints under various environmental conditions. Environments of simulated sea-water at 20°C and 50°C, combined environment of an elevated temperature of 50°C and 90% relative humidity (RH), and combined condition of cyclic thermal load ranging from 20°C and 50°C and constant 90% RH were included in the test matrix. Results showed that the main failure mode of joints was CFRP delamination. After exposed to harsh environment, all the specimens showed a degradation in the strength and stiffness.

Nguyen et al. [40] also studied the effect of temperatures around the glass transition temperature ( $T_g$ ) of adhesive on the mechanical properties of CFRP-steel joints. Joint specimens with different bond lengths under temperatures between 20°C and 60°C were tested. It was found that the effective bond length of joints increased with the temperature. In addition, when the temperature increased, the joint stiffness and strength showed a significant drop. The decrease in the joint strength may be related to the degradation of adhesive. For the specimens under a lower temperature, CFRP delamination failure was mainly observed. When the temperature was near or greater than  $T_g$ , joints failed through cohesive failure.

Nguyen et al. [41] examined the time-dependent behavior of joints under various conditions, including different load levels (i.e. 80%, 50% and 20% of the ultimate load measured at room temperature), constant temperatures from 35°C to 50°C and a cyclic thermal loading between 20°C and 50°C. It was found that joints at a constant tensile load less than the ultimate load and a constant temperature exhibited an obvious time-dependent behavior (i.e. increase of elongation and decrease of load carrying capacity). The time-to-failure of joints varied because of the joint strength reduction with the time. High temperature or larger applied load resulted in shorter time-to-failure. Also, joint strength degradation is not only a single variable function of temperature but also time-dependent and affected by the thermal loading history.

Nguyen et al. [42] reported the examination of bond characteristics of double strap joints under ultraviolet radiation (UV) for various time periods and only thermal environments without UV. Results revealed that ultimate strain of the epoxy decreased under exposure to UV and associated temperatures. The elastic modulus of the epoxy increased under exposure to UV and temperature. Both UV and temperature had no obvious effects on the tensile strength and stiffness of carbon fiber specimens and CFRP specimens. The CFRP delamination was the main failure mode of all the joints. Effective bond length increased with exposure to UV and temperature. UV exposure alone did not affect the mechanical performance of joints.

Heshmati et al. [43] studied the mechanical behavior of FRP-steel joints under hydrothermal aging conditions under 20°C deionized water (DW), 20°C 5% NaCl salt water, 45°C relative humidity (RH), 45°C DW and 45°C 5% NaCl salt water. It was found that the presence of moisture for less than a critical period can increase the joint strength. However, prolonged exposure to the same moisture content degrades the load-carrying capacity of the joint. The CFRP material exhibited very low diffusion and lower moisture uptake. The elastic modulus of adhesive significantly decreased with increasing moisture content.

Agarwal et al. [44] investigated the effect of mechanical and environmental loads on the behavior of CFRP/steel joints, including sustained load only under ambient temperature, wet thermal cycling only, both sustained-load and wet thermal cycling and both sustained load and thermal cycling in dry conditions. The results showed that the debonding failure at the interface between the steel and the adhesive was the dominant failure mode observed in the specimens under wet thermal cycling (with or without sustained load). This proved that wet thermal cycling mainly degraded the steel-adhesive interface. Moreover, it was revealed that it was mainly the moisture

that degraded steel-adhesive interface and not thermal cycling. Thus, CFRP-steel joints with water-proof sealant to prevent moisture ingress in the bonded region was suggested.

Sahin et al. [45] presented the effect of elevated temperatures on the bond behavior of CFRP-steel joints. Tensile tests were conducted on the specimens of joints under two different temperatures of 25°C and 50°C. The results revealed that the tensile strength and stiffness of adhesive decreased at 50°C compared to those at 25°C. Debonding observed at the CFRP-adhesive or steel-adhesive interfaces was the main failure mode. When the temperature increased, the failure location shifted from the adhesive-CFRP interface to the adhesive-steel interface. Also, increasing the temperature increased the debonding load.

Borrie et al. [46] reported the bond behavior of CFRP/steel joints under 5% NaCl solution at 20°C, 40°C and 50°C. It was found that bond strength decreased after environmental conditioning. Saline solution alone did not cause losses in strength. However, when the temperature increased to near or above  $T_g$  of epoxy, it dramatically affected the bond strength of joints.

Heshmati et al. [47] investigated the mechanical properties of CFRP-steel double strap joints under various environmental conditions, including immersion in distilled water at 20°C and 45°C, immersion in de-icing salt solution at 20°C and 45°C and exposure to 95% relative humidity at 45°C. It was found that long-term immersion in saltwater contributed to more damaging to the strength of CFRP material than immersion in distilled water. After immersion at 20°C, the joints did not exhibit any obvious changes on the strength. When the temperature increased, the failure mode shifted from cohesive to interfacial or interlaminar failure modes.

Bai et al. [48] studied the environmentally-assisted degradation of the bond behavior exposed to harsh environments such as elevated temperatures, seawater, cyclic temperature, humidity and ultraviolet radiation. The results showed that the load-carrying capacity of joints decreased at temperature near to and greater than  $T_g$  of the adhesive. After exposure to simulated seawater for one year, the residual strength of joint decreased 20-30%. The residual strength and stiffness showed little decrease after exposure to combinations of temperature and humidity.

Nguyen et al. [49] studied the mechanical performance of CFRP/steel joints cured under different combination of environmental and loading conditions, including 0% and 35% of the ultimate load and simultaneously exposed to constant temperatures of 20°C and 50°C and different load levels and simultaneously subjected to cyclic temperature between 20°C and 50°C. The

results showed that curing at elevated temperature did not negatively affect the strength of joints. However, the elevated temperature cured joints had an improvement in strength when tested at an elevated temperature. Combination of mechanical loading, cyclic temperature and a constant 90% relative humidity caused significant effects on the mechanical properties of CFRP/steel joints.

It is also important to study the effect of corrosion damage on the performance of CFRP strengthened steel components. Batuwitige et al. [50] evaluated the bond characteristics and environmental durability of degraded CFRP-steel joints. To simulate the accelerated corrosive environment, an electrochemical method was used. For this method, bonded CFRP was regarded as anode and the stainless-steel bar acted as the cathode. They were submersed into the 5% NaCl in a tank. After exposure to this environment for a period of time, the failure mode shifted from steel-adhesive interface debonding to CFRP fiber rupture. The environmental aging negatively affected the load capacity of the joint.

Kabir et al. [51] reported the durability of CFRP strengthened steel circular section members under accelerated corrosion environment. A significant drop was observed in stiffness and strength compared to those of control structures. Due to accelerated corrosion effects, the failure modes changed to rupturing of CFRP and yielding of steel.

Dawood et al. [21] evaluated the effect of severe corrosion environment on the mechanical properties of steel bridges and structures strengthened with CFRPs. The results showed that the environmental exposure caused degradation of the bond, leading to debonding failure between CFRP strips and steel structures. Degradation including severe corrosion of the steel and build-up of corrosion products on the CFRP were noticeably observed. The strength and stiffness showed a significant drop when steel structures strengthened with CFRPs were exposed to corrosion environment for long durations.

Batuwitage et al. [34] presented the results of research program on the durability of CFRP-steel joints in accelerated corrosion conditions. Severe degradation was observed in CFRP materials with higher exposure level. CFRP rupture failure mode was the main failure mode. Large reduction in strength and stiffness was reported due to a combination of degradation of CFRP material and adhesive.

Kim et al. [52] investigated the bond performance of steel structures strengthened with CFRPs under various periods of galvanic current. The results showed that electrochemical reactions resulted in hydrated ferric oxide along the CFRP-steel surface. The rate of corrosion had

an adverse effect on the load-carrying capacity of steel structures strengthened with CFRPs. CFRP-debonding was the dominant failure mode.

### **2.3 Strengthening Steel Members Using CFRP Strand Sheets**

Previous studies mostly focused on the bond behavior between steel plates and either CFRP laminates or CFRP sheets. As discussed in earlier section, small diameter CFRP strand sheets are relatively new form of CFRP and made of bunch of individually hardened fiber strands. Since the CFRP strand sheets consists of small-diameter strands stitched together, they possess gap between the strands that allows each strand to be completely covered by the adhesive material. By this way, the adhesion defects which are caused by the poor impregnation of epoxy hardly occur.

Hidekuma et al. [53] studied the failure modes of steel plates strengthened with small diameter CFRP strand sheets. The results indicated that the rate of debonding was reduced compared to conventional continuous carbon fiber sheets.

Tabrizi et al. [28] investigated the flexural capacity of steel beams and bridges girders strengthened with small diameter CFRP strands. They proved that the CFRP strands can effectively increase the flexural capacity and stiffness, similar to the use of sheets and laminates. Moreover, they have the important advantage of elimination of debonding of the strengthening materials.

Kazem et al. [29] examined the bond characteristics of steel girders strengthened with small diameter CFRP strands. The results demonstrated that the CFRP strands did not show any signs of debonding at large lateral deformation associated with elastic buckling. Despite this promising performance of CFRP strand sheets in strengthening steel structures, the durability of CFRP strand sheets strengthened steel plates has not been studied in the current literature. This study aims to fill this gap.

## **2.4 Galvanic Corrosion**

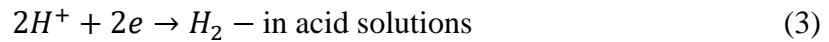
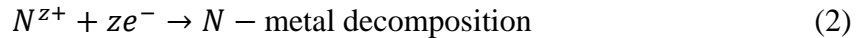
### **2.4.1 Theory**

Corrosion is defined as the degradation of a metal by an electrochemical reaction with its environment. For corrosion to take place, a corrosion cell is needed. Four essential components included in the corrosion cell are anode, cathode, electrolyte and electrical connection. A brief description of each component is provided below:

**Anode**: Anode is the negative terminal of the cell and it is the location where corrosion of metal occurs. Electrons are released at the anode and then move through the wire connection into the cathode. When the metal loses electrons, the ion or insoluble product may be formed. Because the oxidation of metal to an ion with a charge is the basic characteristic of anodic reactions, the process of oxidation in most metals represents corrosion. If oxidation is stopped, the corrosion is stopped. The general expression of anodic reaction is:



**Cathode**: Cathode represented as a positive terminal of a cell. Electrons are consumed at the cathode. The common cathodic reaction is given below:



**Electrolyte**: It is the electrically conductive solution to transfer the ions. Owing to exposure conditions, when moisture combines with salt or other components, it can serve as an electrolyte.

**Electrical connection**: The general reaction process in the electrolyte is shown in Figure 3.

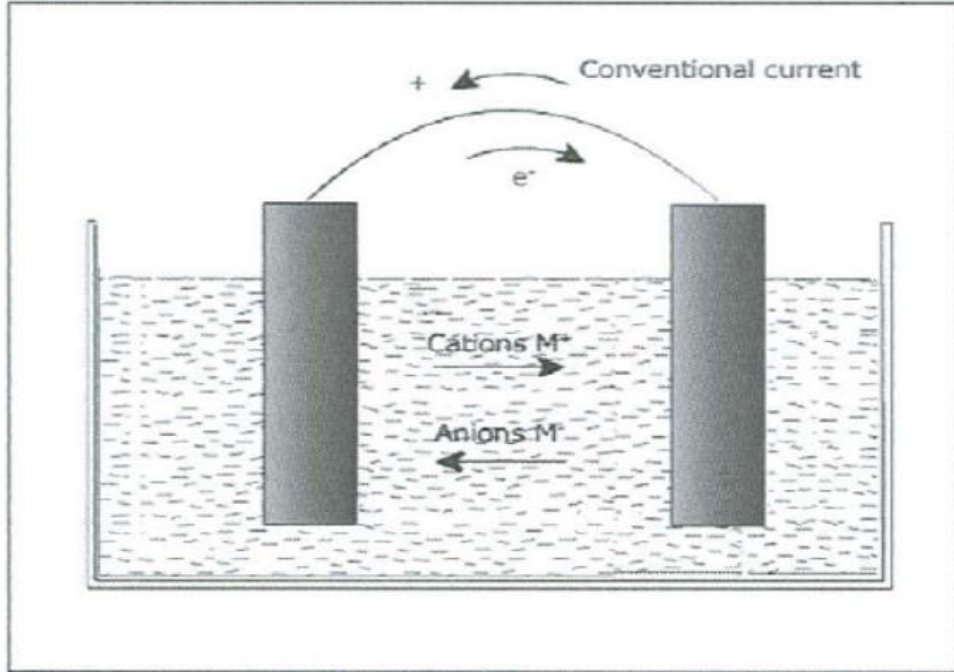


**Figure 3.** Anodic and cathodic processes in a corrosion cell [54]

#### 2.4.2 Faraday's laws of electrolysis

Two laws, proposed by Faraday, are commonly used to estimate the corrosion rate and mass loss rate. The first law states that the mass of primary products formed at an electrode is directly proportional to the quantity of electricity passed. The second law indicates that the mass of different primary products formed by equal amounts of electricity are proportional to the ratio of molar mass to the number of electrons involved with a particular reaction. Based on the two laws, the methods to calculate corrosion rate and mass loss rate are given in the ASTM G102-89 [55]. The equations are summarized as follows:

$$CR = K_1 i_{cor} EW / \rho \quad (5)$$

$$MR = K_2 i_{cor} EW \quad (6)$$

where  $K_1$  and  $K_2$  are conversion constants and are, respectively, and equal to  $3.27 \times 10^{-3} mm \frac{g}{uA} - cm - year$  and  $8.954 \times 10^{-3} mm \frac{g}{uA} - cm - year$ ,  $\rho$  is the density of the

anode,  $EW$  is the equivalent weight, and for steel is taken as 27.92, and  $i_{cor}$  is the current density in  $\mu\text{A}/\text{cm}^2$ , calculated by Eq. (7):

$$i_{cor} = \frac{I_{cor}}{A} \quad (7)$$

where,  $I_{cor}$  is the measured electrical current, in  $\mu\text{A}$ , and  $A$  is the exposed surface area of the metal specimen, in  $\text{cm}^2$ .

### **3. EXPERIMENTAL DESIGN AND TESTING**

This chapter describes the materials and equipment used in this research. The experimental tests conducted in this study are also discussed.

#### **3.1 Tensile Characterization of Materials**

##### **3.1.1 Adhesive**

A blue-colored two-components epoxy resin, FB-E7S, was used as the adhesive in this study, which was chosen because of their inherent durability and high degree of resistance to chlorides, moisture, and freeze-thaw cycles. In order to determine the mechanical properties of this adhesive, tests on adhesive specimens were conducted. Specimens were fabricated using a plastic mold designed to enable demolding of the specimens without damage. The cross-section dimensions of the specimens were 13 mm × 4 mm. These dimensions of the dog bone-shaped specimens were decided according to ASTM D638-10 [56]. A total of six specimens were manufactured as shown in Figure 4. Also, to make the adhesive fully cured, all the specimens were left for one week at room environment. The tests were conducted by using the MTS 810 hydraulic machine with a maximum capacity of 22 kips in the displacement-control mode and at a constant loading rate of 0.5mm/min. Figure 5 showed the test set-up of the specimens in the MTS. The MTS data acquisition system was used to record the displacement and force data. To obtain the stress of adhesive, the recorded force values were divided by the cross-sectional area of the adhesive. The strains were measured using a laser extensometer. In addition, because the epoxy was viscous, air bubbles were easily formed during mixing and casting of the adhesive. The presence of these air bubbles may reduce the measured tensile strength and modulus of adhesive. However, this is acceptable as it represents the practical field applications.

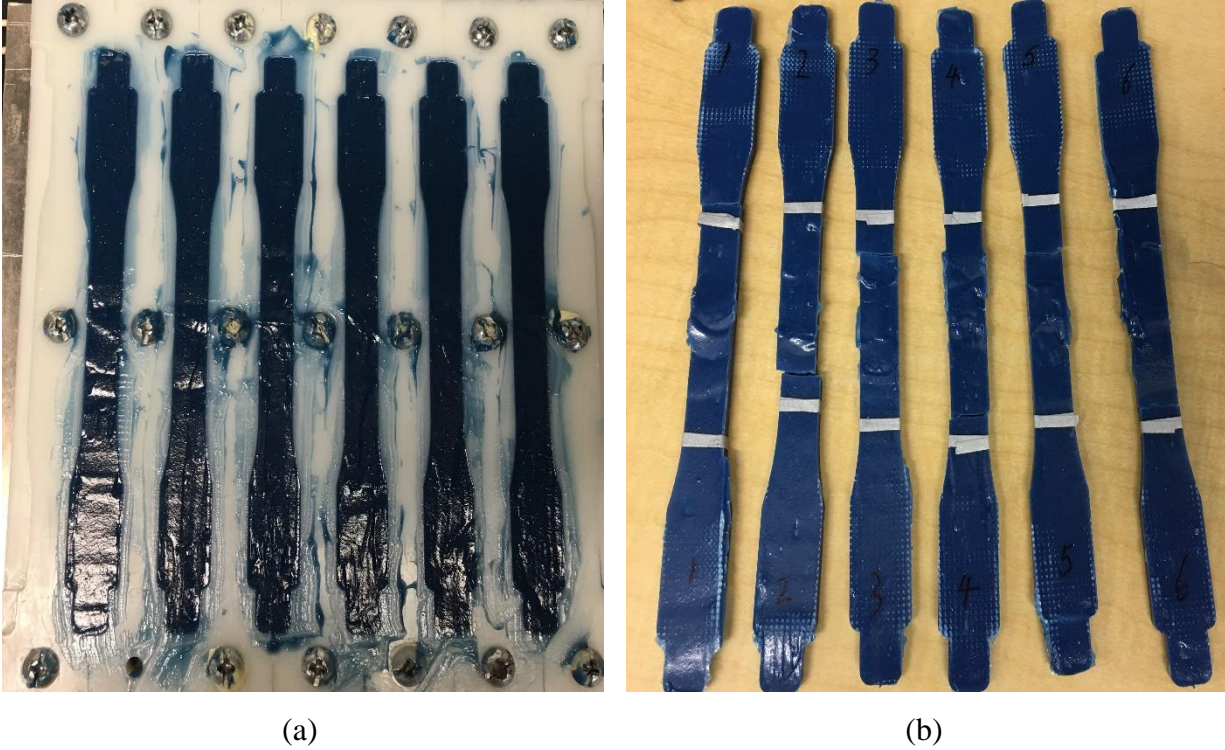


**Figure 4.** Adhesive tensile test samples: (a) in molds, (b) after curing

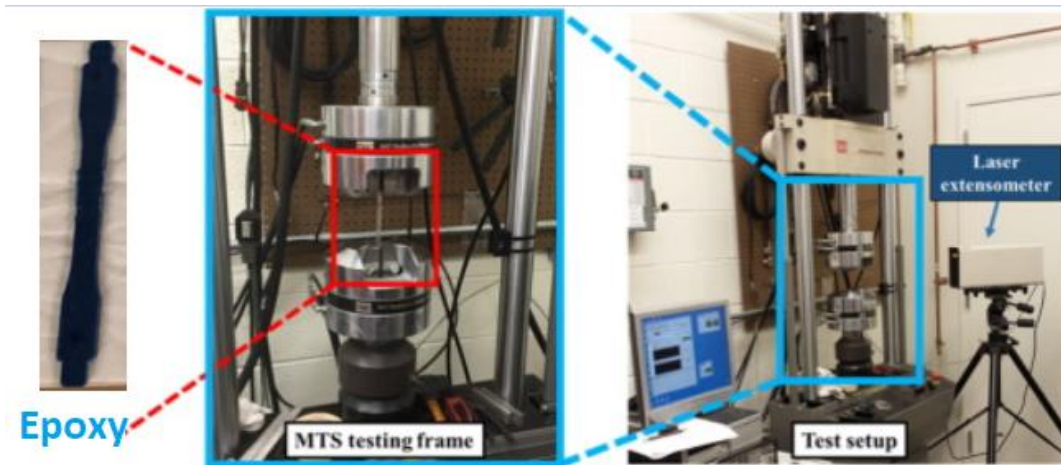
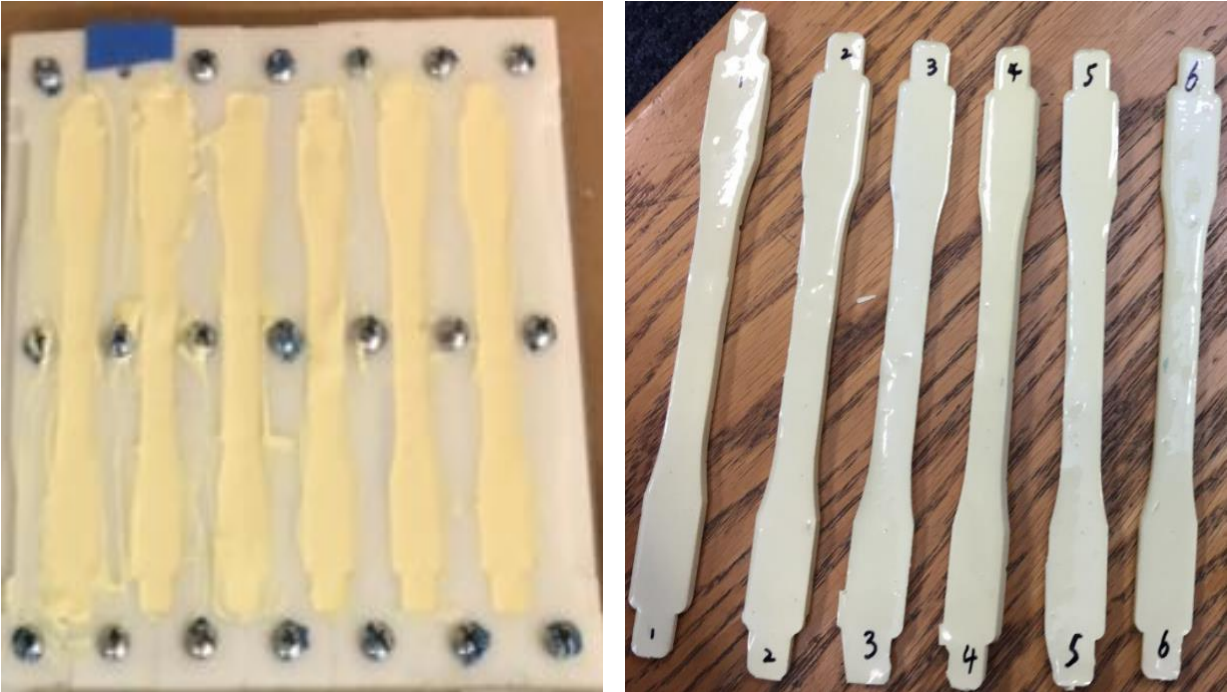


**Figure 5.** Test set-up for adhesive

### 3.1.2 Primer

A yellow colored primer, FP-WE7W, was used as the primer in this study, as shown in Figure 6. It was used to protect the steel surface from corrosion by preventing the direct contact

between CFRP and steel plates. The same fabrication and testing procedures with adhesive were utilized to determine the mechanical properties of this primer. The dimensions of the specimens were also the same with that of adhesive described ASTM D638-10 (56). Also, to make primer fully cured, all the specimens were left for one week at room environment according to manufacturers' standards. Different from adhesive is that air voids were not observed during the fabrication of the specimens.



(a) (b)  
**Figure 6.** Primer tensile test samples: (a) in molds, (b) after curing

**3.1.3 Single strand of CFRP**

Six specimens of the individual CFRP strand in accordance with ASTM D3039 [57] were prepared for tensile testing as shown in Figure 7. The tests were also conducted by using the MTS 810 hydraulic machine at a constant loading rate of 0.2mm/min.

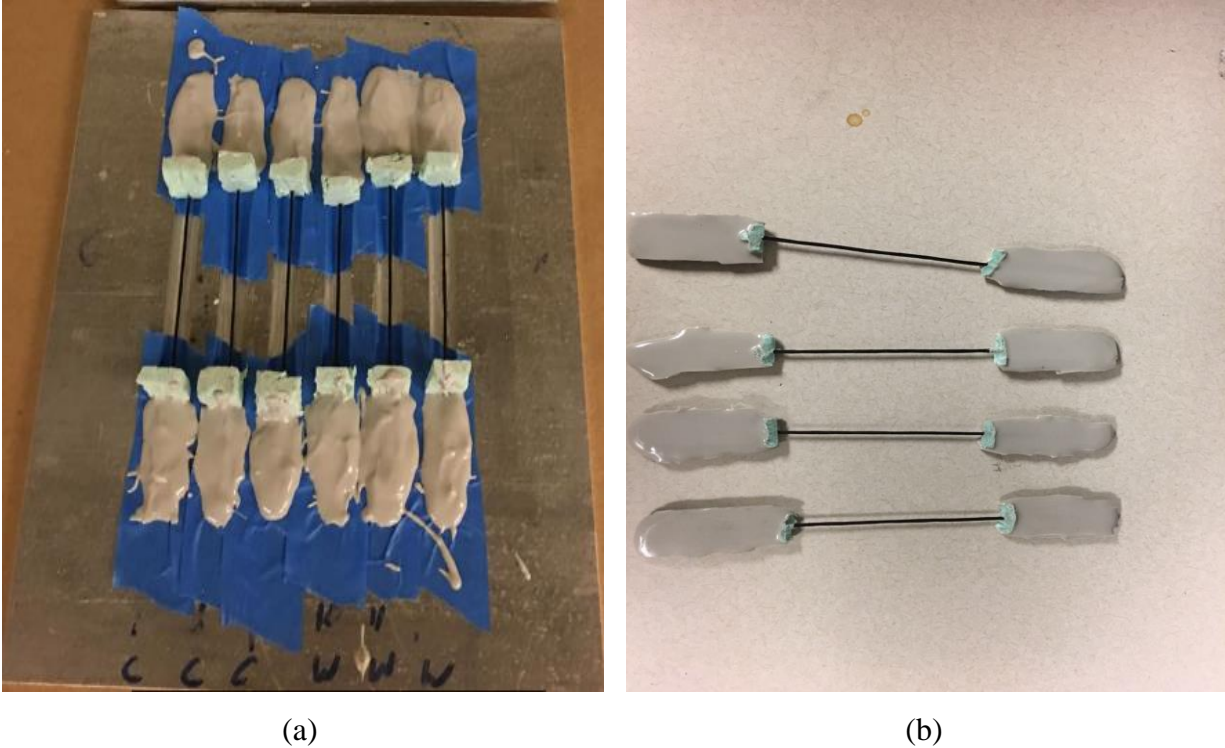


**Figure 7.** Single CFRP strand tensile test samples: (a) in molds, (b) after curing

### **3.1.4 CFRP strand sheets**

To characterize tensile behavior of CFRP strand sheets, aluminum tabs were firstly glued to the ends of each CFRP coupon to prevent the failure occurred in the grips. But the specimens still failed in the grips of testing machine. To solve this problem, CFRP woven sheets were applied to the end of CFRP coupon and the gripping pressure was decreased. With this change, the failure did not occur at the grips and the mechanical properties of CFRP strand sheets were then drawn from the test. The schematic view of CFRP strand sheets with woven sheets or aluminum tabs was shown in Figure 8.

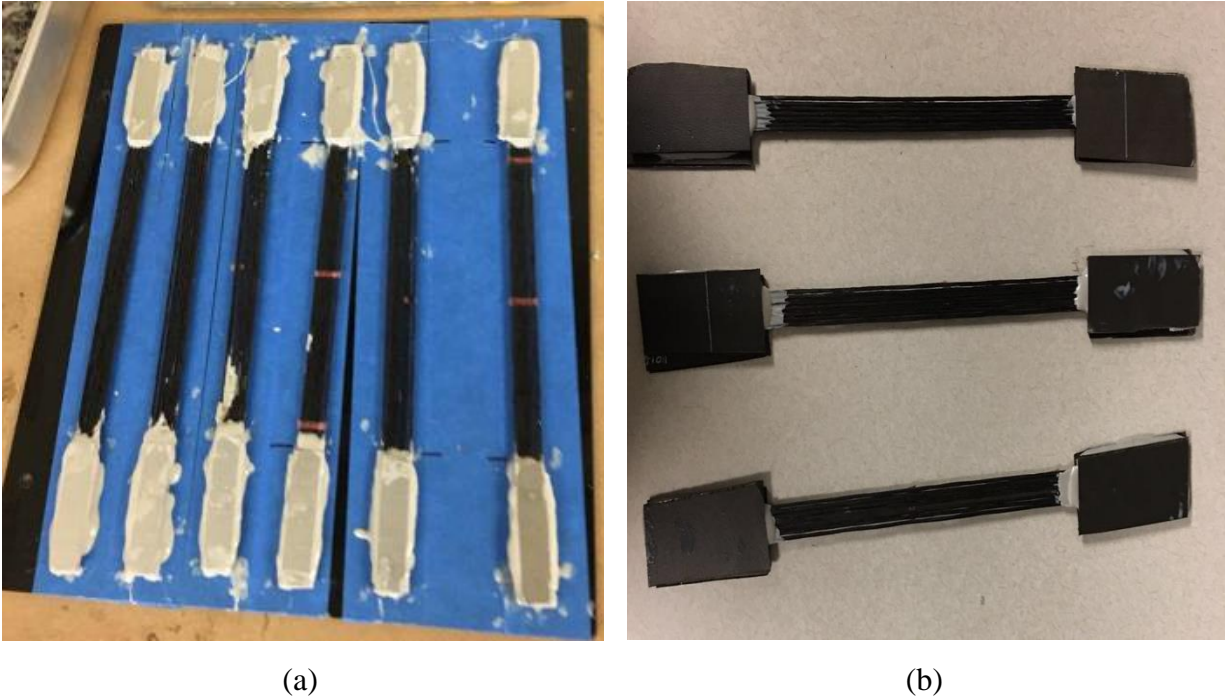


**Figure 8.** CFRP strand sheets (a) with aluminum tabs, (b) with CFRP woven sheet tabs

### 3.2 Fabrication of CFRP-Steel Double Strap Joint Specimens

Double strap joints are mainly applied to investigate the bond behavior between steel plates and CFRP sheets. A schematic view of a typical double strap joint specimen is shown in Figure 9 where the length  $L_b$  is always less than  $L_c$  to aim that the failure occurs on one end only.  $L_b$  was defined as the bond length and  $L_c$  was regarded as the control length. The test specimens consisted of two 9.525-mm-thick and 50-mm-wide steel plates that were bonded together using two 1-mm  $\times$  50-mm CFRP strand sheets. A two 2-mm-thick adhesive layers was used to bond the CFRP materials to the steel surface. Also, the plates were aligned end to end with one another with a 2-mm gap between them to minimize stress transfer through end-to-end bonding of the steel plates. Figure 10 shows the section view of joints and the layout of materials.

Because different thickness profiles of the adhesive layer can significantly affect the bond behavior of double strap joints, preparation of steel-CFRP joints is the most critical step of the testing [58]. To keep all the specimens consistent with the same bond thickness, we adopted a standard fabrication process and three specimens were fabricated simultaneously. To this end, a mold was fabricated shown in Figure 11. This device aims to provide a uniform pressure on the

external surface of the CFRP to bleed out excessive adhesive and air bubbles. The device is also intended to create a uniform thickness of adhesive which could affect the bond behavior. However, the adhesive thickness was not the focus of this thesis, so all tests were conducted with approximately 2 mm of adhesive thickness. Steps to prepare the specimens were described below.

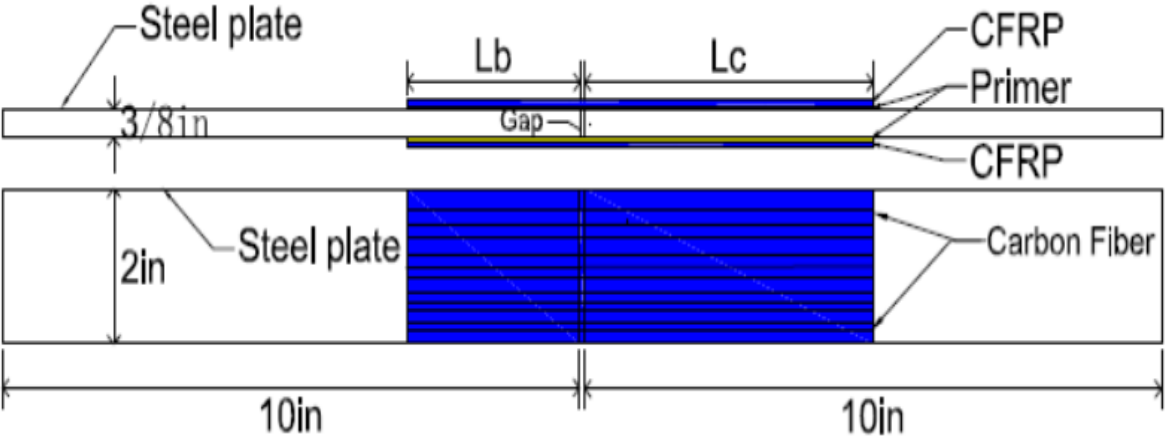


**Figure 9.** Schematic diagram of CFRP-steel double strap joint

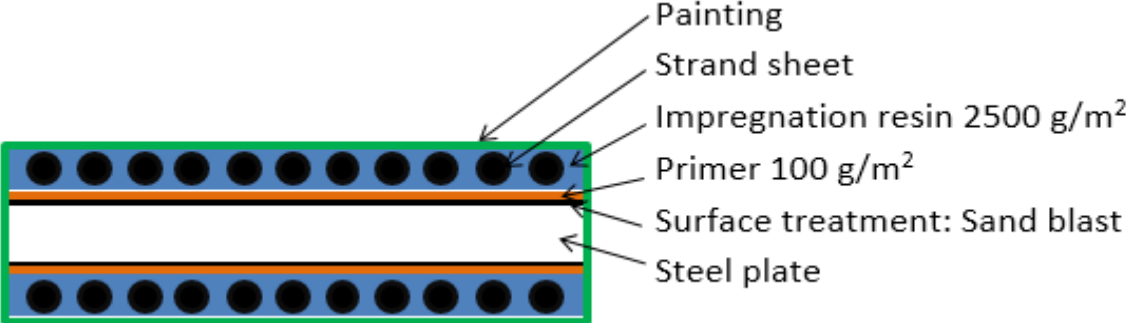
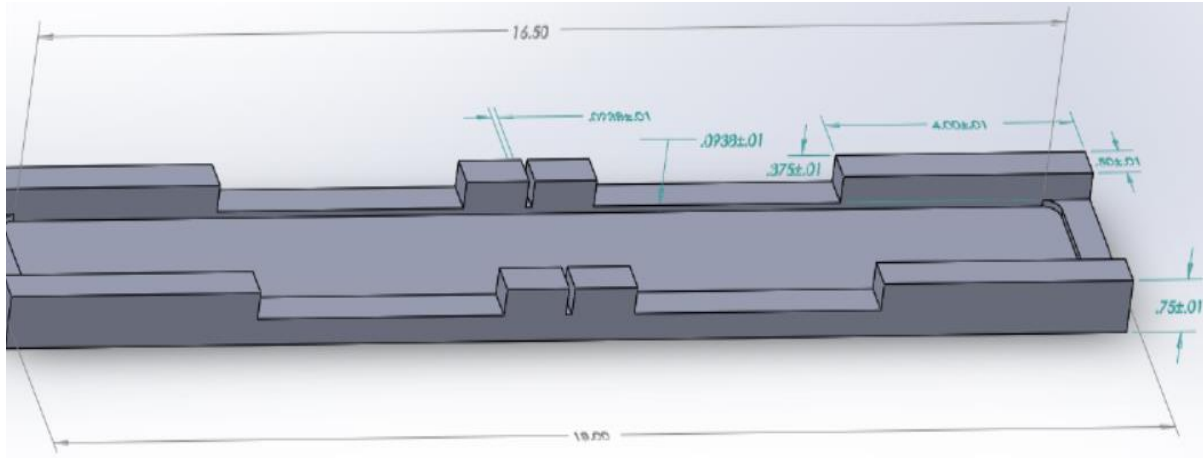
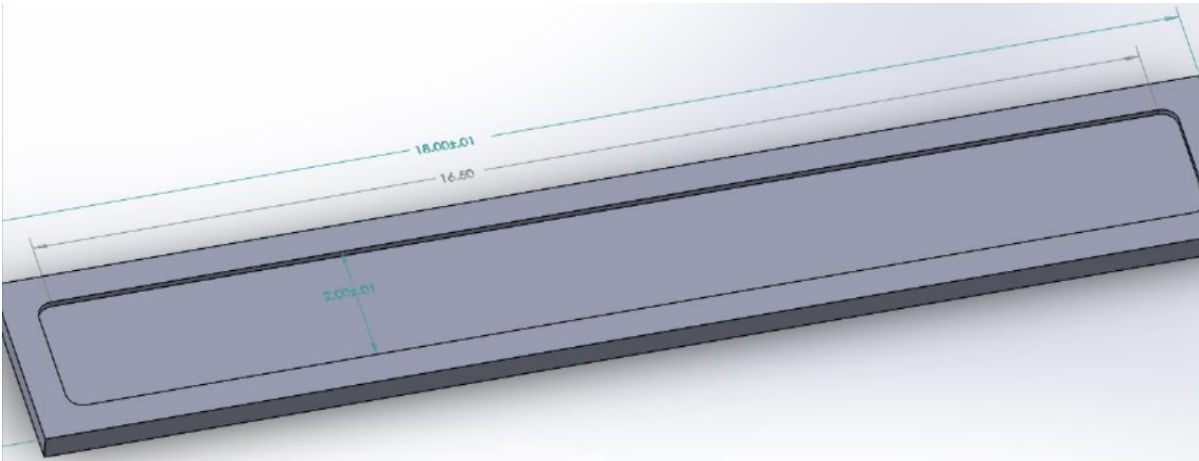


**Figure 10.** Section view of CFRP-steel double strap joint



(a)



(b)

**Figure 11.** Sketches of (a) top and (b) mold molds used in fabrication of double strap joints

### 3.2.1 Preparation of steel plates

Steel plates were cut to dimensions of 10 in × 2 in × 3/8 in by using the hydraulic shear machine. Surface preparation of steel plates is needed to enhance the bond behavior between steel plates and adhesive. The surface of steel plates was prepared to cleaning standard St1/2 according to ISO 8501-01 [59]. First, acetone was used to remove surface dust, grease, and other contaminants. In order to achieve a better mechanical interlocking between steel plates and adhesive, the sandblasting was carried out by applying a garnet grit (garnet size of 60) in a compressed air regulator and a nozzle angle of approximately 45°. After sandblasting, acetone was

re-used to clean the steel surface to remove any fine abrasive dust that may remain attached on the steel surface. The contrast of steel surface before and after cleaning was shown in Figure 12. After the surface treatment, the steel plates were left to dry completely before applying a coat of primer to the surface of the steel. In addition, to minimize the possibility of recontamination or oxidation of the steel surface, the initial primer was applied within the shortest time which was less than four hours. That is largely because too long of a time after the surface of preparation can result in adhesive failure between steel substrate and the adhesive [58].

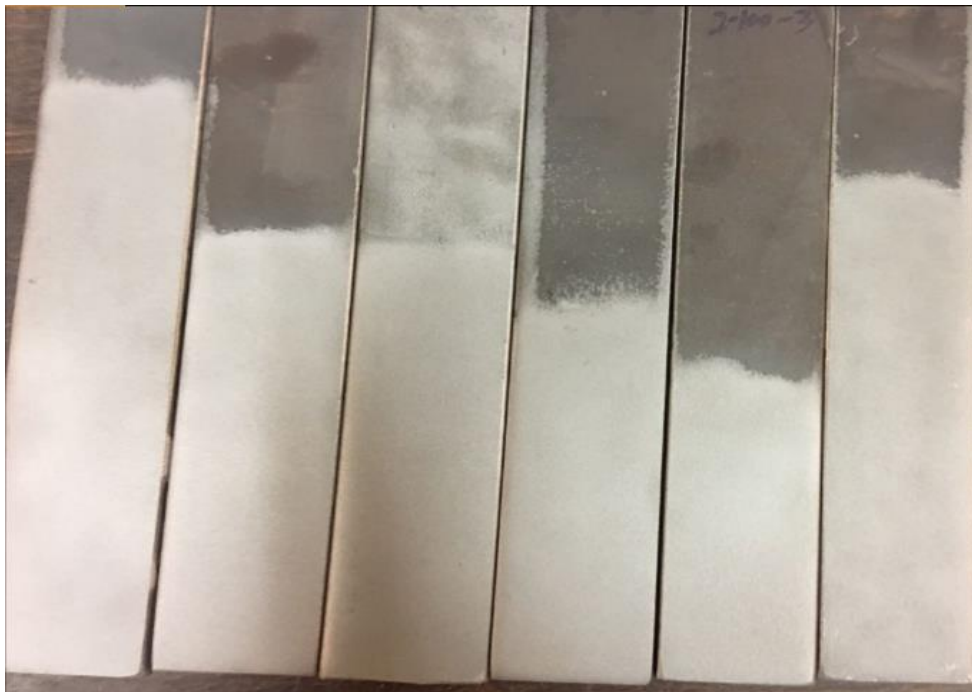


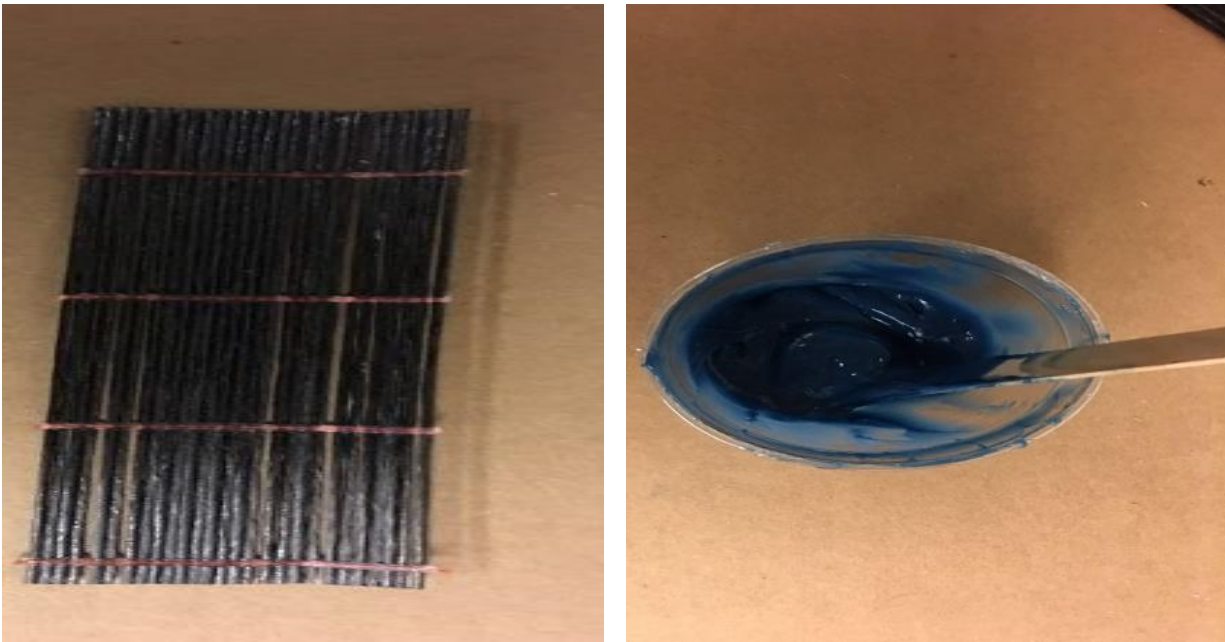
**Figure 12.** The contrast of steel surface before and after cleaning

### **3.2.2 Application of primer on the steel surface**

Primer was mixed according to the manufacturer's instructions and one thin coat of primer was applied uniformly on one side of the steel plates. The assembled specimen was then cured at room temperature for 12 hours. Then, a thin coat of primer was applied on the other side of steel plates after which the specimen was cured at the room temperature for additional 12 hours. The amount of primer resin was suggested to be  $100\text{g/m}^2$ , which yielded very thin layer of coating.

### **3.2.3 Bonding CFRP sheets**

The CFRP strand sheets were cut by scissors based on the required size and the adhesive was mixed by a 2:1 resin-to-hardener mixing ratio by weight according to the manufacturer's specifications as shown in Figure 13. Then, CFRP specimens were formed at the bottom and top mold during the bonding process by impregnating CFRP sheets with epoxy resin as shown in Figure 14. Figure 15 shows that two separate steel plates were put on the surface of epoxy at the bottom mold. Next, when steel plates were aligned in position in a jig at the bottom mold, the bottom mold and the top mold were then connected together as shown in Figure 16. Finally, clamping was applied to improve the bond between steel plates and CFRP and ensure the uniform thickness of adhesive by using the clamping device as shown in Figure 17. After that, the excessive adhesive along the plate was scraped off. The final specimen is shown in Figure 18.



(a)

(b)

**Figure 13.** Preparation of materials(a) carbon fiber strand sheets, (b) epoxy

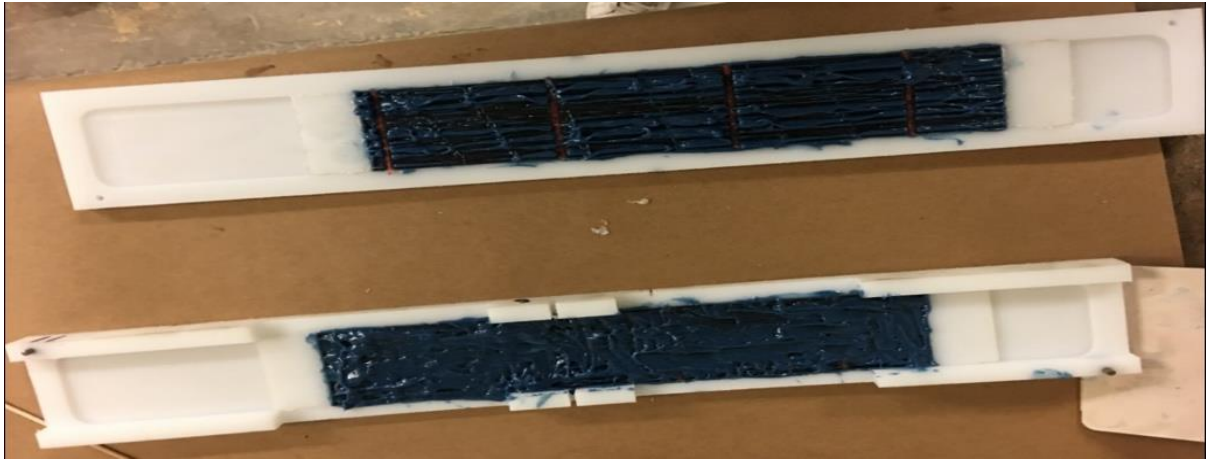


**Figure 14.** Placing CFRP sheet to top and bottom mold



**Figure 15.** Placing steel plates on surface of epoxy



**Figure 16.** Connecting the top and bottom mold



**Figure 17.** Placing the mold into the clamping assembly



**Figure 18.** Applying pressure to molds by clamping

### 3.2.4 Curing condition

Specimens of CFRP-steel double strap joints were cured at room temperature for at least seven days prior to testing.

### 3.3 Test Matrix

Double strap joints with unequal bond lengths were fabricated (i.e.  $L_b$  was always 50mm shorter than  $L_c$ ) to make the specimens fail at the shorter bond length [40]. In addition, to fully utilize the strength of the CFRP material, the effective bond length ranging from 75 mm to 175 mm was selected for the tensile tests. A total of 36 specimens were prepared as listed in Table 1. Three specimens were selected per condition to account for the potential uncertainty. Each specimen was named as BL $x$ -Cy-i. The first three characters represent the different bond length and the fourth or fifth letter describes the exposure duration (i.e. CS=control specimens (no exposure), A=24 h exposure, B=48 h exposure and C=72 h exposure). The last letter stands for the “i-th” specimen. For example, the specimen BL75-A-1 refers the first specimen with a bond length of 75 mm under the exposure duration of 24 h.

**Table 1.** Test matrix

Specimen identification	Exposure duration (hour)	Repetition
BL75-CS	0	3
BL75-A	24	3
BL75-B	48	3
BL75-C	72	3
BL125-CS	0	3
BL125-A	24	3
BL125-B	48	3
BL125-C	72	3
BL175-CS	0	3
BL175-A	24	3
BL175-B	48	3
BL175-C	72	3

The first goal of the testing was to investigate the effect of exposure duration that indicates severity of corrosive conditions on the effective bond length of the double strap joints. After each

exposure duration, specimens with different bond lengths were tested in tension until failure. The results from this investigation provided the effective bond lengths of the joints at the four designated exposure durations. The second goal was to study the failure modes and the degradation of double strap joints in terms of stiffness and strength at different exposure durations.

### **3.4 Accelerated Corrosion Environment**

To simulate the accelerated corrosion environment, direct current (DC) was applied on the steel plates by means of DC supply power. Different electric currents were utilized through the double strap joints for each bond length, which represented an approximate current density of  $7500 \mu\text{A}/\text{cm}^2$  and was within the range of current density used in the literature [60]. The current density was obtained by dividing the total current by the surface area of the double strap joints submerged in the solution of 5% NaCl. The corrosion cells were made with plastic tanks, anodes, cathodes and electrolytes. The double strap joints served as the anode, which the stainless-steel strips were regarded as the cathode. They were connected in parallel to the positive and negative phases of the DC power supply respectively. In addition, two resistors of one ohm were also connected to assure that the constant current flowed between the anode and cathode by measuring the volt of resistors. For the double strap joints, the bare steel plate was protected with marine paint to assure corrosion observed in the bonding area. The joints were then placed in the pipe filled with simulated 5% NaCl. In addition, only the joints' shorter bond length was submerged in the pipe filled with simulated 5% sodium chloride. To minimize the evaporation of the solution, any gaps between the pipe were tightly sealed. The schematic view and the laboratory test set-up of the accelerated corrosion cell were shown in Figure 19 and Figure 20. The joints exposed to accelerated corrosion conditions for 24h, 48h and 72h are studied during this thesis. These durations were determined based on Faraday's law resulting in 5%, 10% and 15% mass loss in bare steel samples. When the exposure time was achieved, all the specimens were cleaned according to ASTM G1[61].

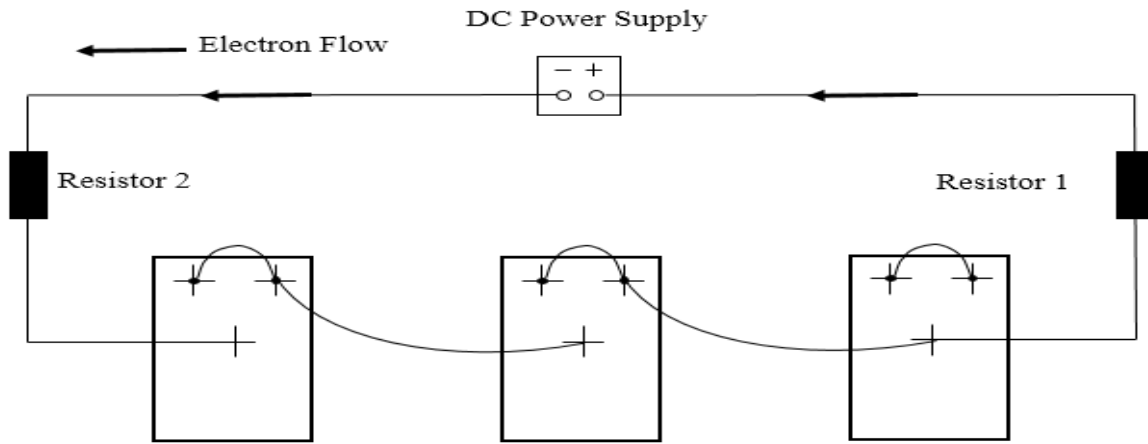


**Figure 19.** Typical layout of accelerated corrosion series circuit [60]

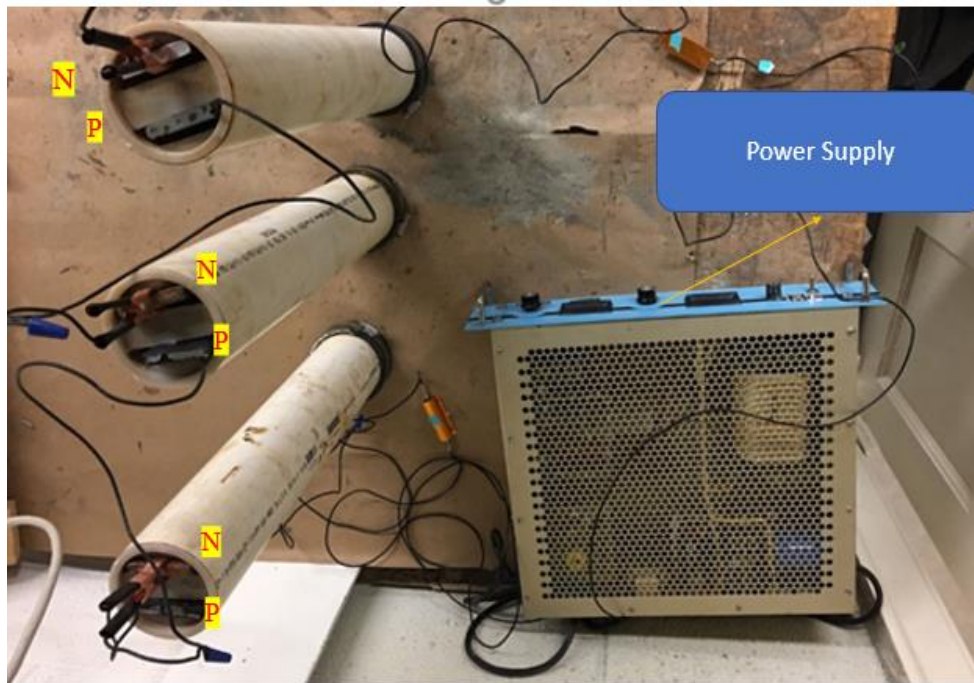


**Figure 20.** Schematic view of accelerated corrosion series circuit

### 3.5 Test Set-up

Double strap joint specimens were tested in tension to failure at a constant displacement rate of 0.1 mm/min using the MTS testing machine with a capacity of 55 kips as shown in Figure 21. Mechanical grips were used at each end of the specimen to minimize the initial slip. Load and displacement readings for each increment were recorded by using the MTS data acquisition system. In addition, a MTS laser extensometer was also used to monitor the relative displacement. The gauge length of 115 mm was constant for all the specimens. To measure the slip, one reflection tape was attached on the CFRP surface on one side and the other tape was attached on another side. The relative movement of the two tapes was captured by the laser extensometer, which can be treated as the total slip of CFRP.

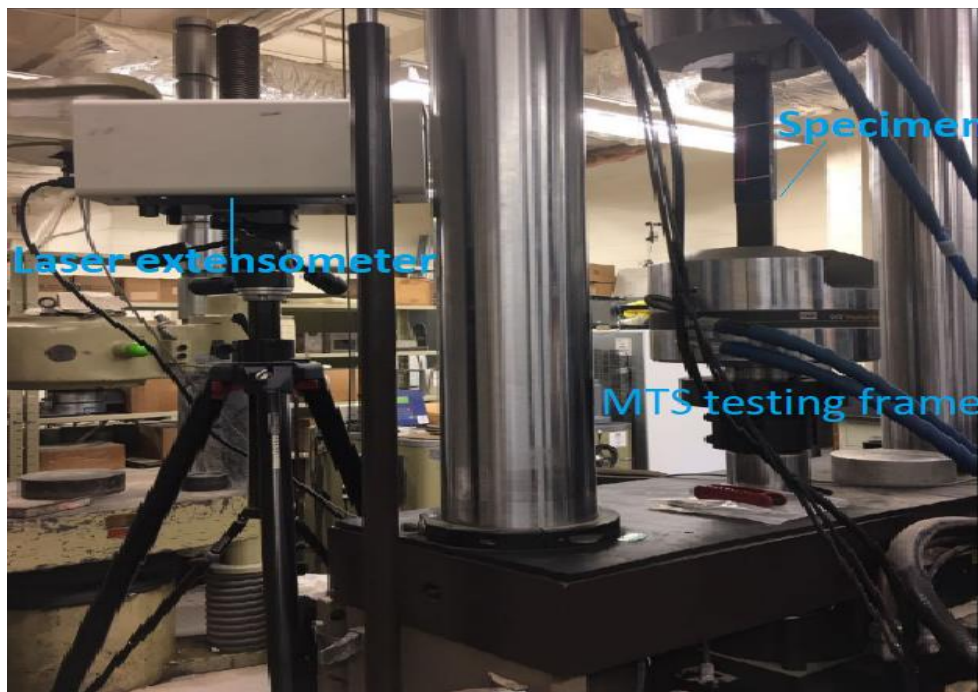


**Figure 21.** Test set-up

## 4. EXPERIMENTAL RESULTS

### 4.1 Mechanical Characteristics of Individual Components

The primer, CFRP and adhesive are the primary materials used in this experimental program. Based on the appropriate ASTM standards, each of the materials was tested to determine their mechanical properties. The testing results are presented in the following sections.

#### 4.1.1 Tensile response of adhesive

Figure 22 shows the stress-strain curve of four epoxy specimens tested under uniaxial tensile loads. The stress was calculated as the recorded force divided by the cross-section area and the strain was measured using a laser extensometer. An average tensile strength of 27.46 MPa was obtained for the FB\_E7S epoxy resin. All of the coupons failed in a brittle manner due to rupture.

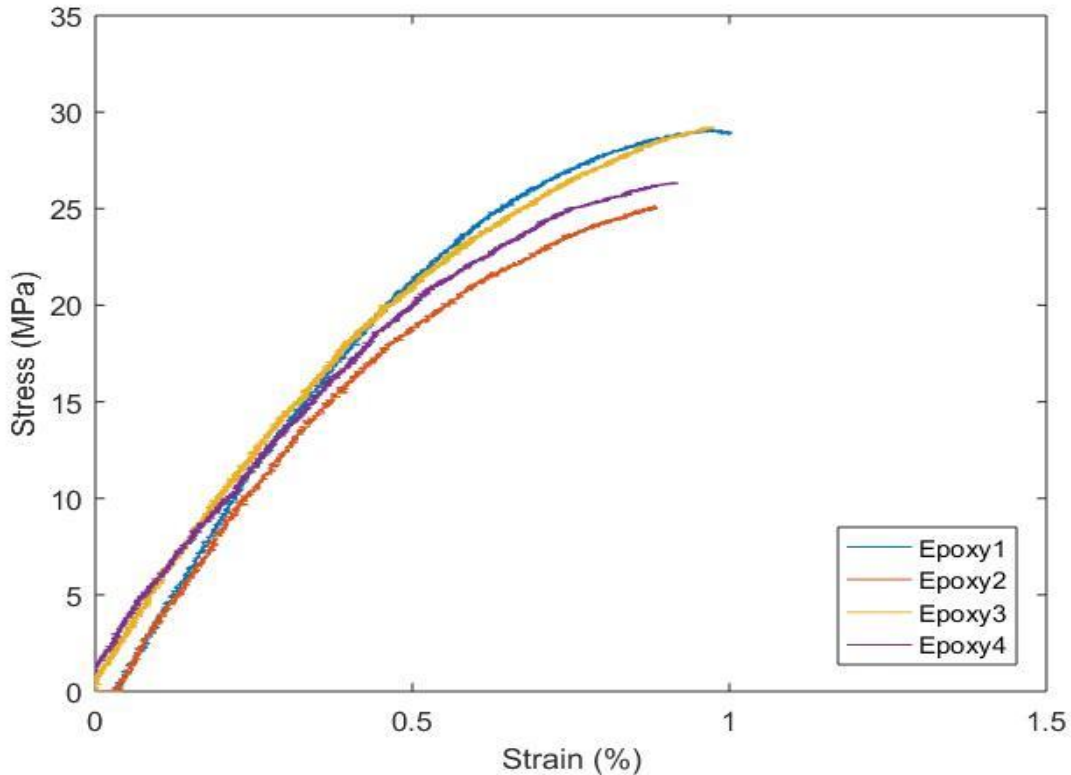


**Figure 22.** Tensile stress-stain behavior of the epoxy

#### 4.1.2 Tensile response of primer

By conducting the tensile tests on primer, the relationship between the stress and strain of seven primer specimens was obtained and shown by Figure 23. An average tensile strength of 21.87 MPa was obtained for the primer FP\_WE7W.

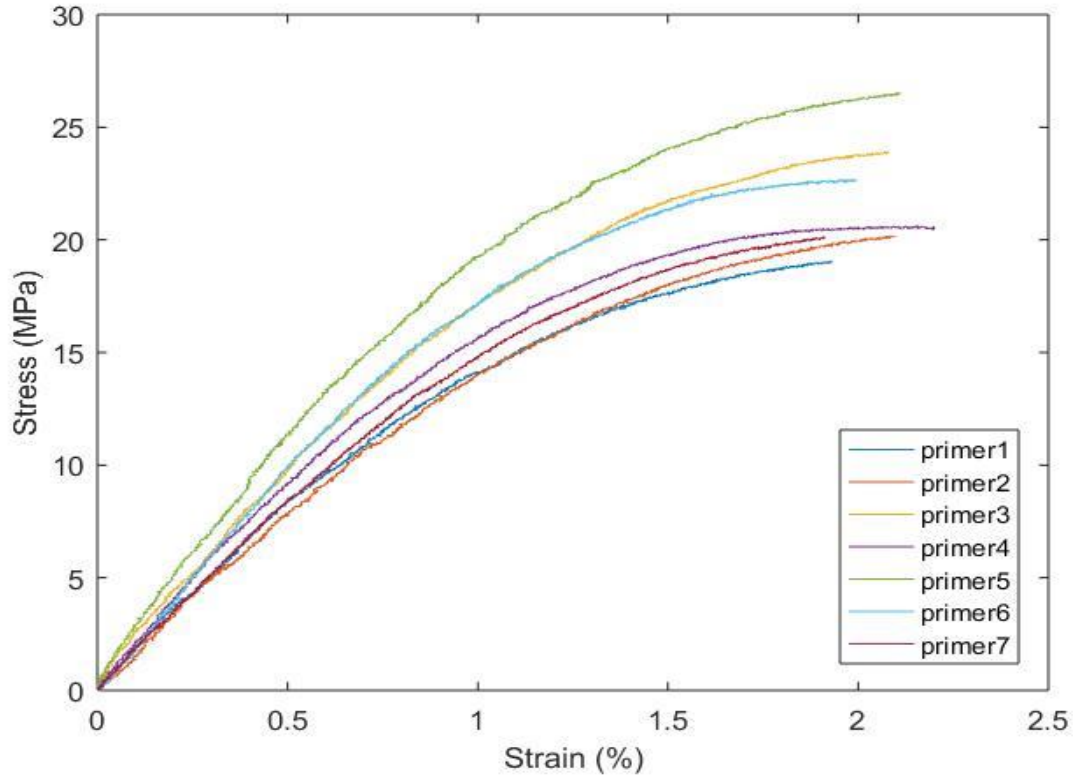
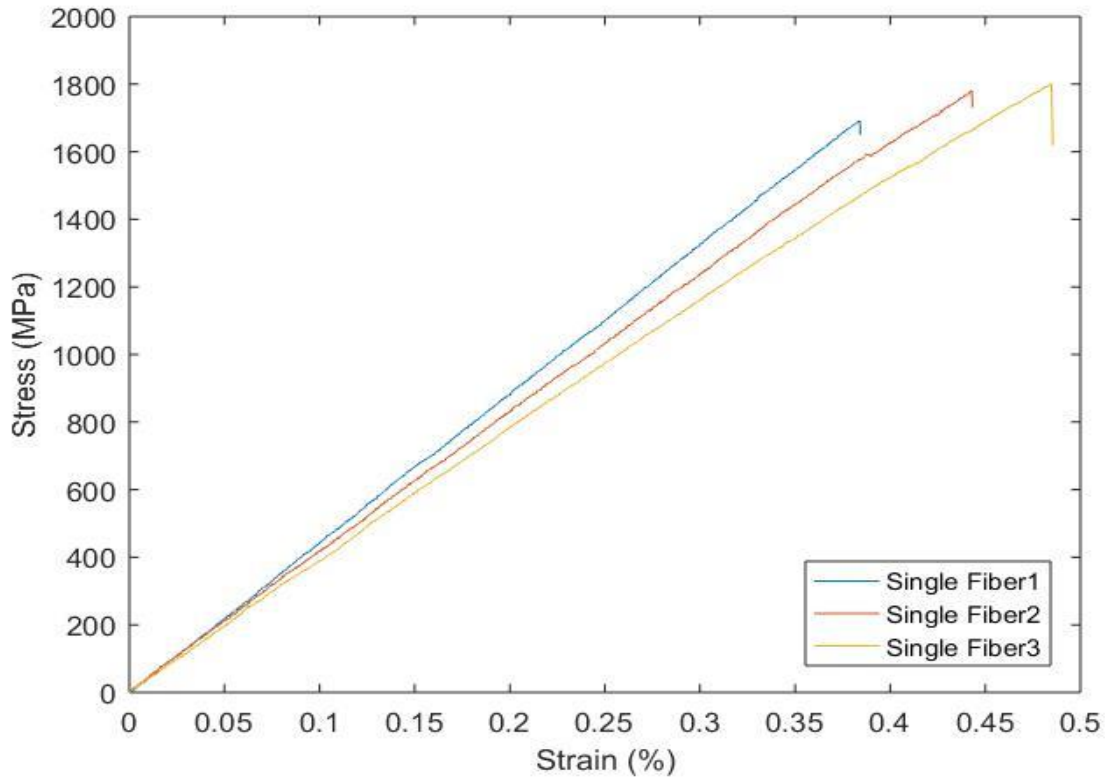


Figure 23. Tensile stress-stain behavior of the primer

#### 4.1.3 Tensile response of individual CFRP strand

The stress-strain relationship of individual CFRP strand was shown in Figure 24. An elastic modulus of 407.83 GPa and average tensile strength of 1758 MPa were obtained for the CFRP strand. All of the coupons failed due to the rupture of CFRP.



**Figure 24.** Stress and strain curve for single CFRP strand

#### **4.1.4 Tensile response of CFRP strand sheets**

This test was performed at a constant cross-head displacement rate of 0.5 mm/min. To prevent the coupons being crushed in the grips of the testing machine, CFRP woven sheets were glued to the ends of each FRP coupon prior to testing. The stress-strain relationship for CFRP strand sheets was shown in Figure 25. The CFRP strand sheets reached an ultimate strength of 2698 MPa and ultimate strain of 0.96%.

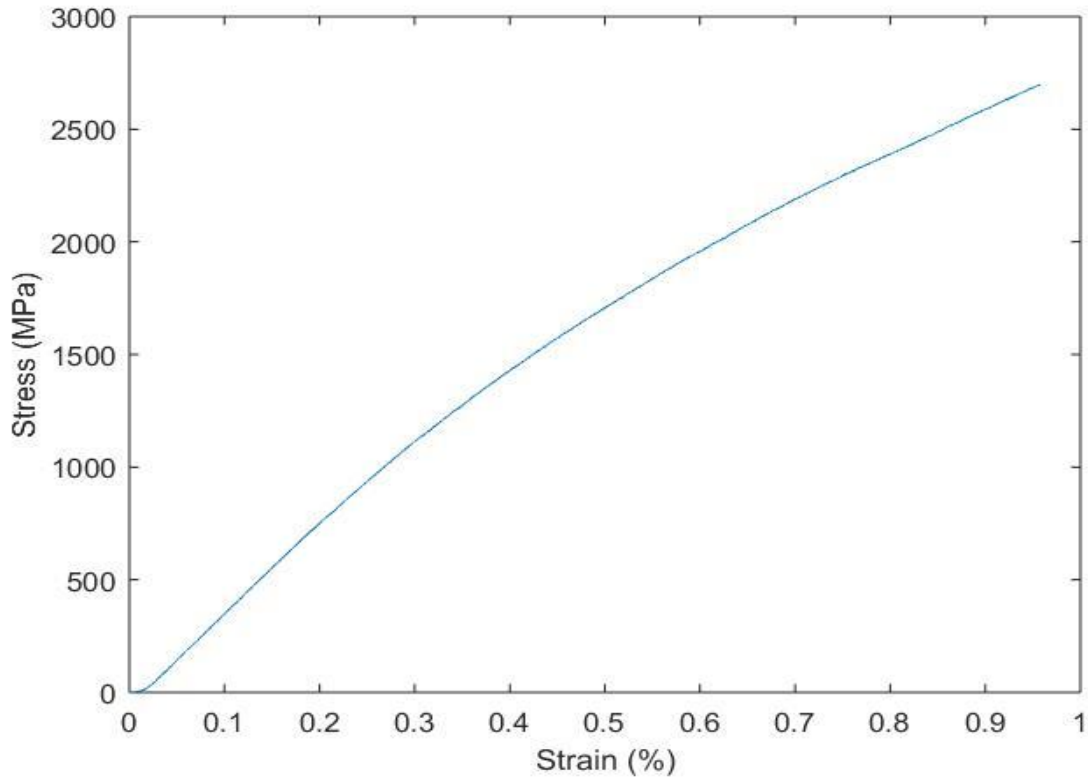


**Figure 25.** Stress and strain curve for CFRP strand sheets

#### 4.1.5 Summary of Tensile Tests

After tensile testing for all the specimens, the average measured mechanical properties were shown as in Table 2.

**Table 2** Material properties of steel, CFRP strand, epoxy and primer

	Steel	CFRP	Epoxy	Primer
Elastic modulus (GPa)	190	407.83	2.96	1.08
Tensile strength (MPa)	448	1758	27.46	21.87
Yield stress (MPa)	345	-	-	-
Tensile strain (mm/mm)	0.022	0.004	0.01	0.02

## 4.2 Specimen Characteristics After Accelerated Corrosion Exposure

### 4.2.1 Characterization of rusts and rust formation

When the specimens were removed from the conditioning tank, noticeable corrosion of steel was inspected. It can be seen that a significant color change caused by the deposition of corrosion products appeared in the CFRP layer. Rusts with brown colors were observed due to the corrosion of steel in the 5% sodium chloride solution. For example, for BL75-B, the surfaces showed clear color degradation and brown rusts formed on the steel plates with the marine paint as shown in Figure 26. As Tamura et al. [62] described, oxidization of iron occurred at the anode to dissolve  $\text{Fe}^{2+}$  and dissolved oxygen was reacted at the cathode to form  $\text{OH}^-$ . Finally,  $\text{Fe}(\text{OH})_2$  was formed during this chemical reaction between the anodes and cathodes. In addition, even though the edges of specimens were protected with marine paint, they still exhibited more corrosion damage than others as shown in Figure 27. It also showed that the surface area and mass of the specimens gradually decreased with the increase of exposure duration. However, the mass loss was less than the theoretical calculation based on the Faraday's Law. For example, specimens with a bond length of 125 mm exposed to the solution for 24 h (BL125-A) only resulted in an average 0.8% mass loss. This phenomenon proved that the primer and adhesive did work to protect the steel plate from corrosion.

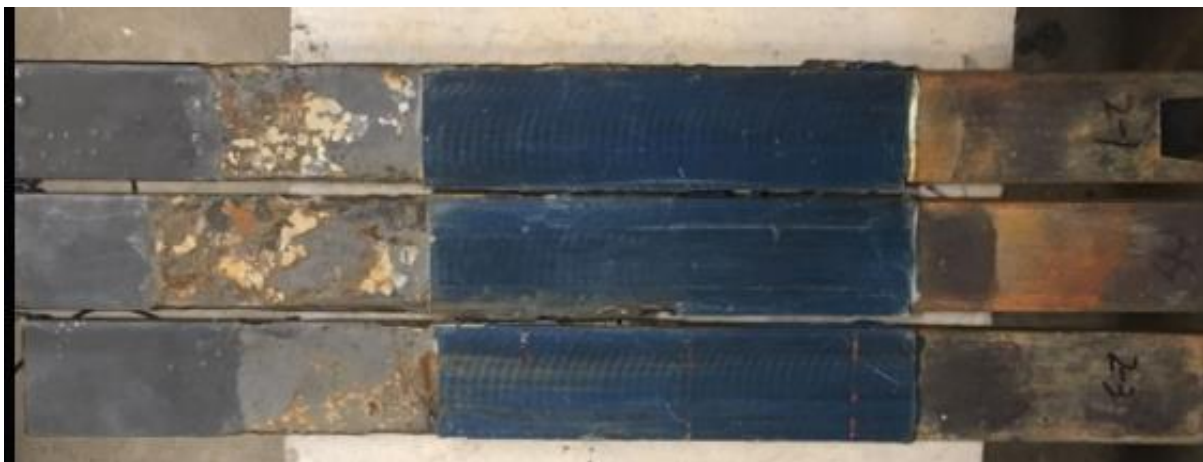


**Figure 26.** Color transformation for BL75-B



**Figure 27.** Corrosion damage of edges of BL75-B

#### **4.2.2 Corrosion rate and mass loss rate**

To evaluate the corrosion rate (CR) and mass loss rate (MR) of the joints, the weights of the specimens were measured by using a scale with 0.1 mg accuracy before the test. At the end of the test, their weights were also measured after a sequence of cleaning procedures according to ASTM G1[54]. Table 3 shows the measured mass. Figures 28 and 29 show the measured corrosion rate and mass loss rate as a function of time. They were calculated according to the Faraday's Law. For example, for the BL75-24, it corroded as an average corrosion rate of 90.49 mm/year and the mass lost as an average mass loss rate of 1945.03 g/m<sup>2</sup>d. The variation of corrosion rate or mass loss rate for different exposure durations was not significant, however larger values were observed for the shorter bond lengths. This is largely because that the progression of corrosion was affected due to the accumulated rust formed over a steel surface and the protection of primer.

**Table 3.** Variation of physical properties with time

Test category	Exposure time	Mass loss (g)
BL75-A-1	24	13.6
BL75-A-2	24	12.7
BL75-A-3	24	9.8
BL75-B-1	48	16.6
BL75-B-2	48	11.3
BL75-B-3	48	19
BL75-C-1	72	27.6
BL75-C-2	72	27.4
BL75-C-3	72	27.5
BL125-A-1	24	17.3
BL125-A-2	24	15.6
BL125-A-3	24	19.5
BL125-B-1	48	42.7
BL125-B-2	48	16.9
BL125-B-3	48	10.8
BL125-C-1	72	17.7
BL125-C-2	72	61.7
BL125-C-3	72	77.8
BL175-A-1	24	26.6
BL175-A-2	24	20.91
BL175-A-3	24	16.9
BL175-B-1	48	56.5
BL175-B-2	48	30.8
BL175-B-3	48	11.7
BL175-C-1	72	66
BL175-C-2	72	23.9
BL175-C-3	72	15.8

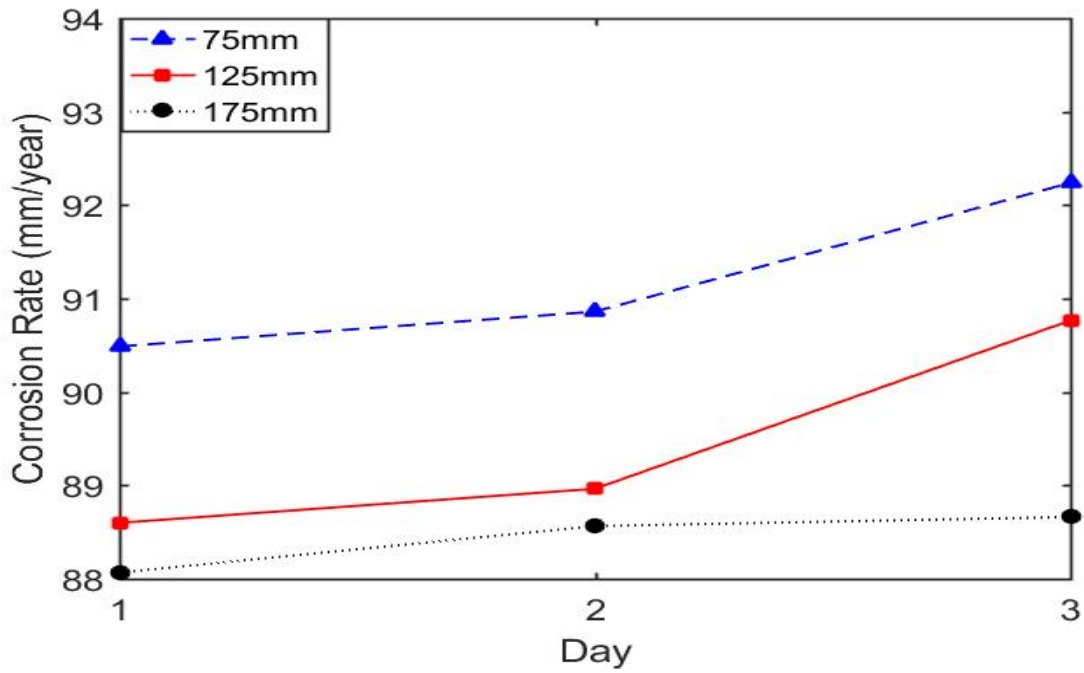


**Figure 28.** Variation of corrosion rate with exposure duration

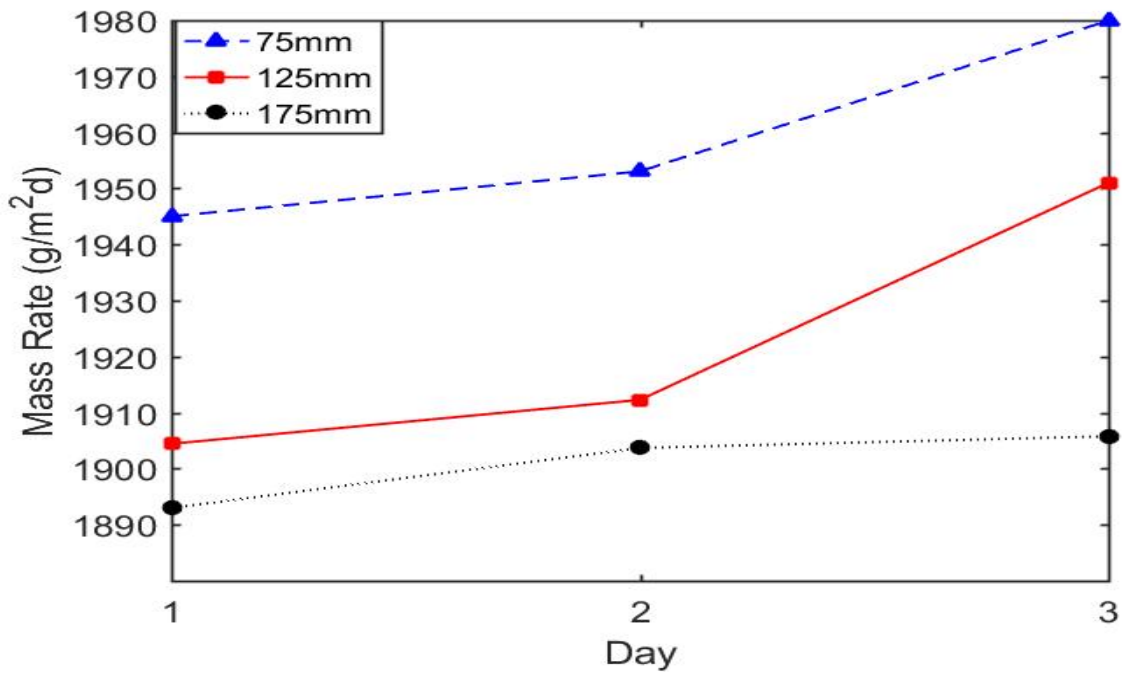


**Figure 29.** Variation of mass loss rate with exposure duration

### **4.3 Tensile Test Results on CFRP-Steel Joints**

#### **4.3.1 Load-displacement curves**

Figures 30 to 33 show the relationship between load and joint displacement for BL75, BL125 and BL 175 specimens at different exposure duration. In particular, Figure 30 shows the load-displacement curve for the control specimens (i.e. no exposure) with different bond lengths; Figures 31 to 33 show the load-displacement curve for the specimens with bond length of 75 mm, 125 mm, and 175 mm, respectively and with exposure durations of 1, 2, and 3 days. The loads applied to each specimen increased with displacement until the ultimate load was reached, after which the load suddenly decreased and the CFRP rupture occurred. It can be seen that the joint ultimate load decreases as the aging time in the corrosive solution increases. At some regions, the response was highly nonlinear, indicating CFRP composite damage. For BL75 specimens, the average of ultimate tensile load was about 93.5 kN at normal conditions. When the exposure duration increased to 24h, 48h or 72h, the ultimate tensile load dropped by 4.5%, 13.8% and 26.8%, respectively. For BL125 specimens, a similar trend was observed: the average ultimate tensile load dropped by 4% to 20% when the exposure duration reached to 3 days. For BL175 specimens, the ultimate loads of the joints showed a decrease of 3.5%, 11.85% and 16.9% at increasing exposure durations. In addition, it was also noticed that the ultimate load capacity decreased when debonding failure occurred at one side.

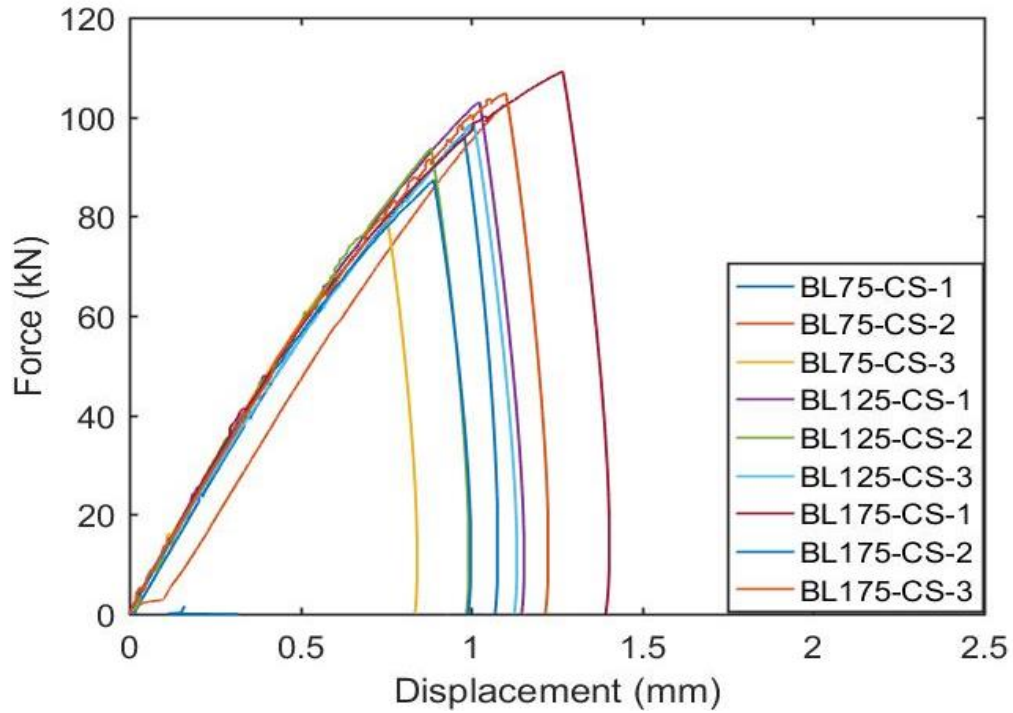


**Figure 30.** Load-displacement curve for specimens BL75-CS, BL125-CS and BL 175-CS

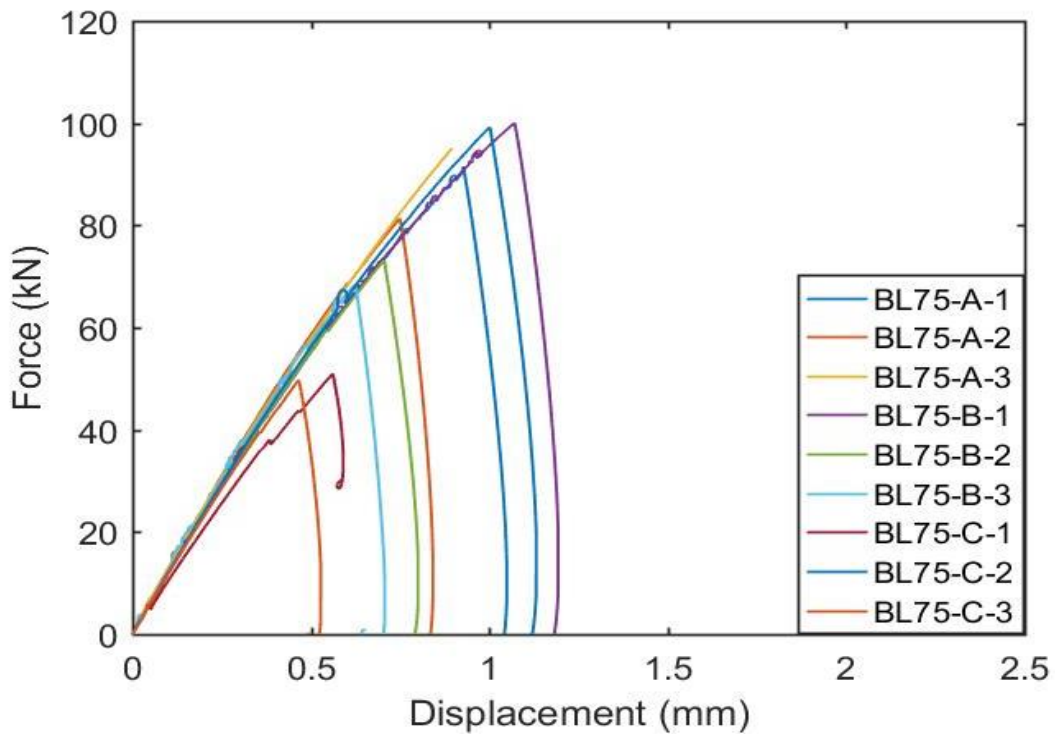


**Figure 31.** Load-displacement curve for specimens BL75-A, BL75-B and BL75-C

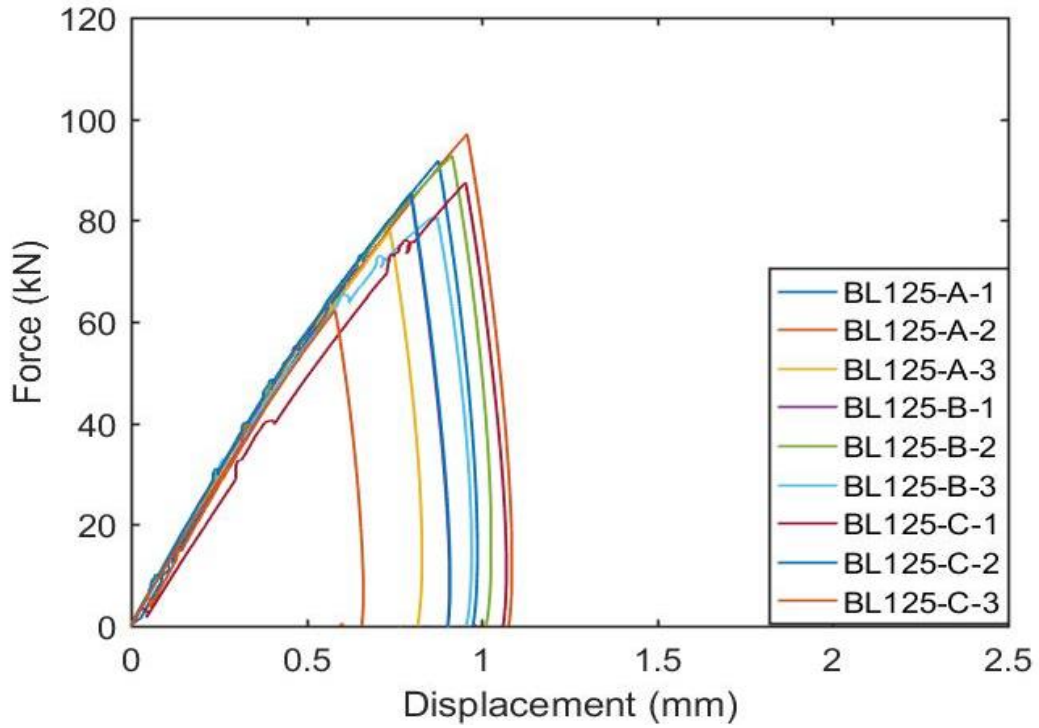


**Figure 32.** Load-displacement curve for specimens BL125-A, BL125-B and BL125-C

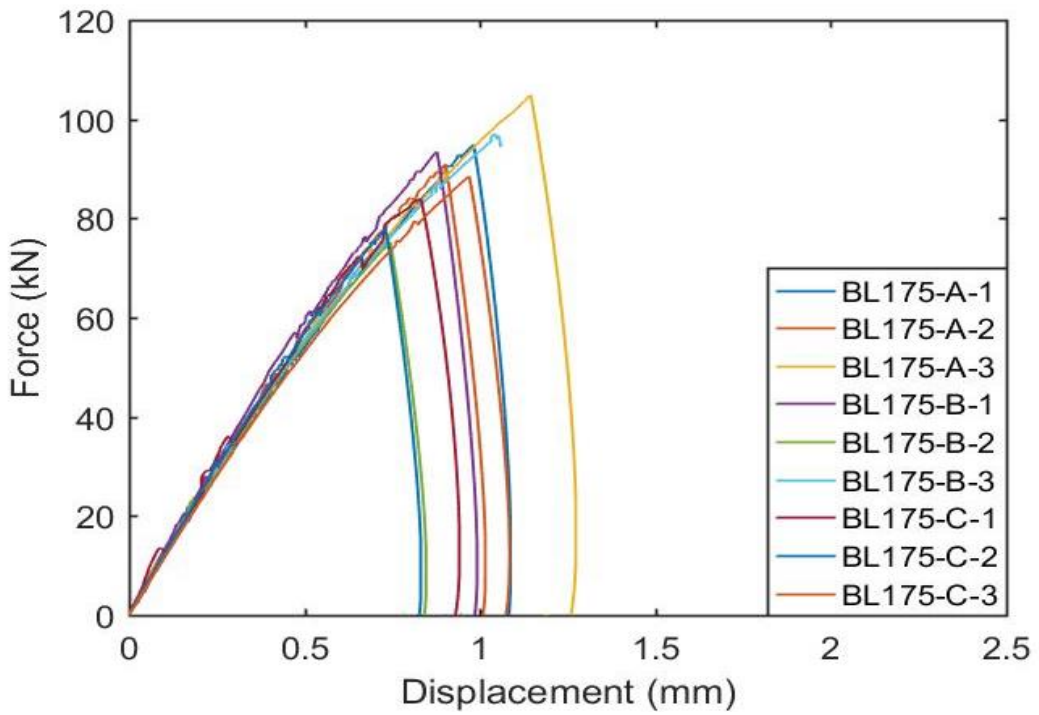


**Figure 33.** Load-displacement curve for specimens BL175-A, BL175-B and BL 175-C

### 4.3.2 Effect of corrosion on joint stiffness

The joint stiffness is defined as the initial slope of the load-displacement curve and it is the ratio of the applied load to the corresponding displacement (kN/mm). The relationship between the stiffness and exposure duration for double strap joints is shown in Figures 34 to 336 for specimens with bond lengths of 75 mm, 125 mm, and 175 mm, respectively. Error bars in these figures represented the range of experimental results. Figure 37 provides the comparison of the stiffness-exposure time relationship for BL75, BL125 and BL175. In this regard, BL75-C specimens exhibited a 19.8% stiffness reduction and BL125-C showed a 4.6 % stiffness reduction compared with control specimens. BL175-C specimens, on the contrary, resulted in a 9% stiffness gain. Given the scatter of the stiffness data, we can see a minimal variation of the measured stiffness for all the tested specimens regardless of the bond detail or the exposure duration. Considering that the stiffness of the double strap joints mainly depends on the stiffness variations of the adhesive and the fact that the adhesive layer did not grade, this result can be justified. This also confirmed that accelerated corrosion has no significant effects on the joints stiffness.

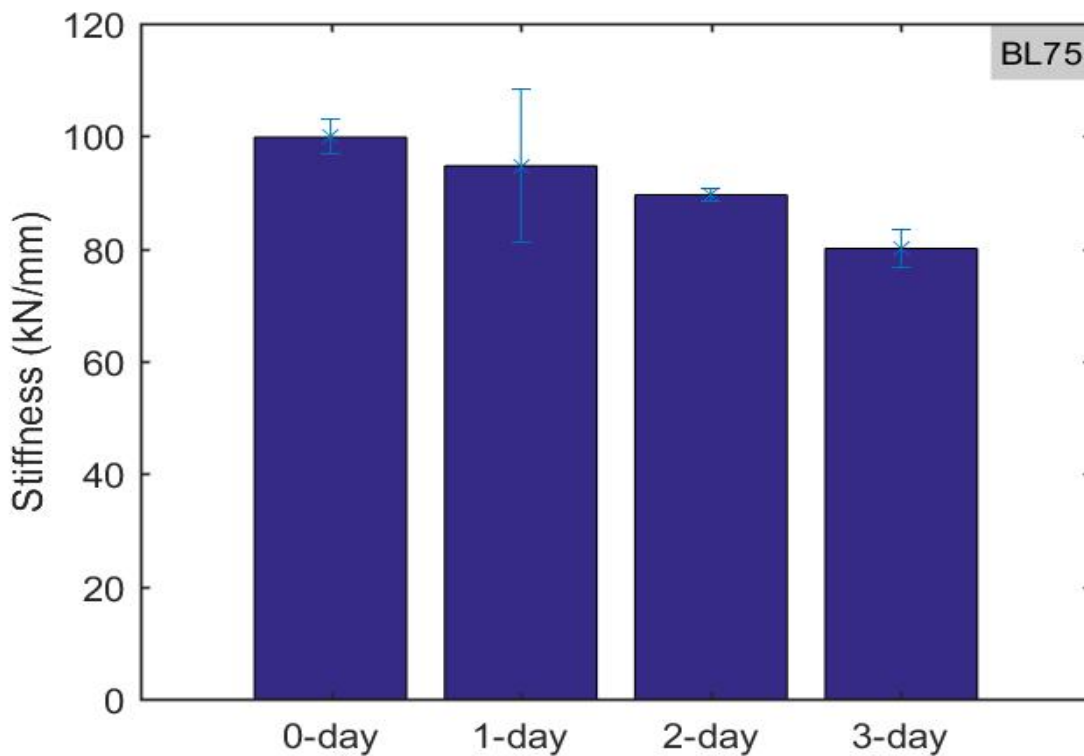


**Figure 34.** Stiffness-exposure time relationship for specimen BL75

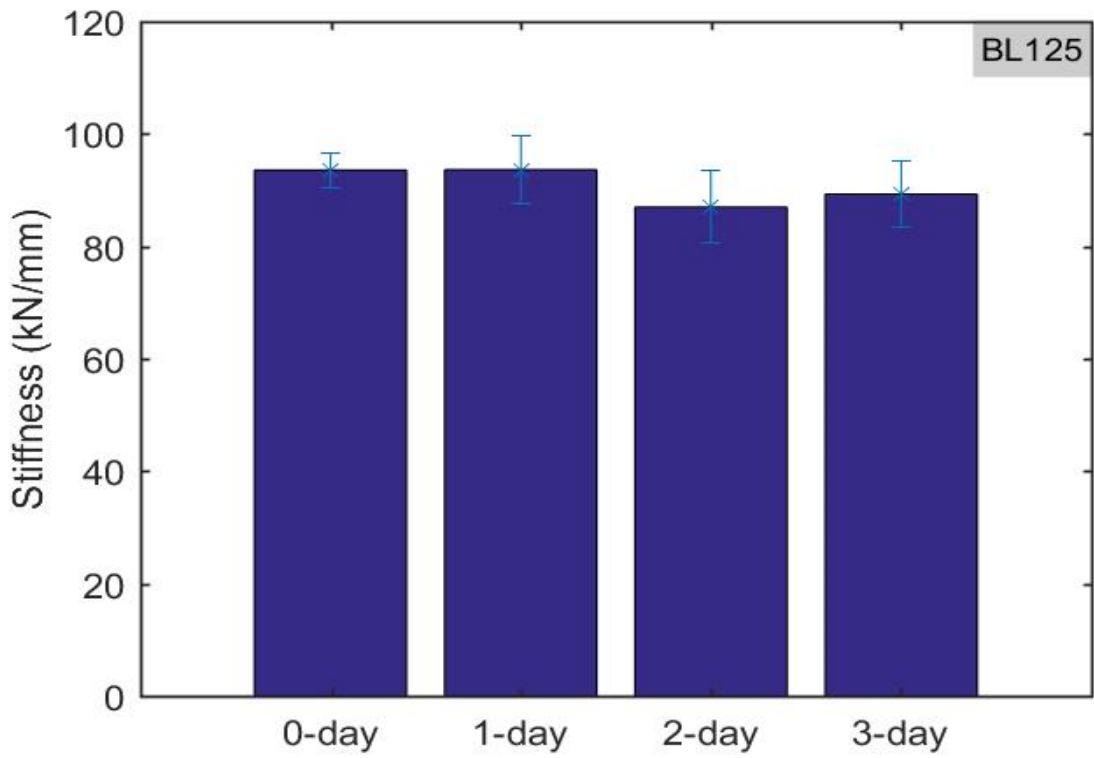


**Figure 35.** Stiffness-exposure time relationship for specimen BL125

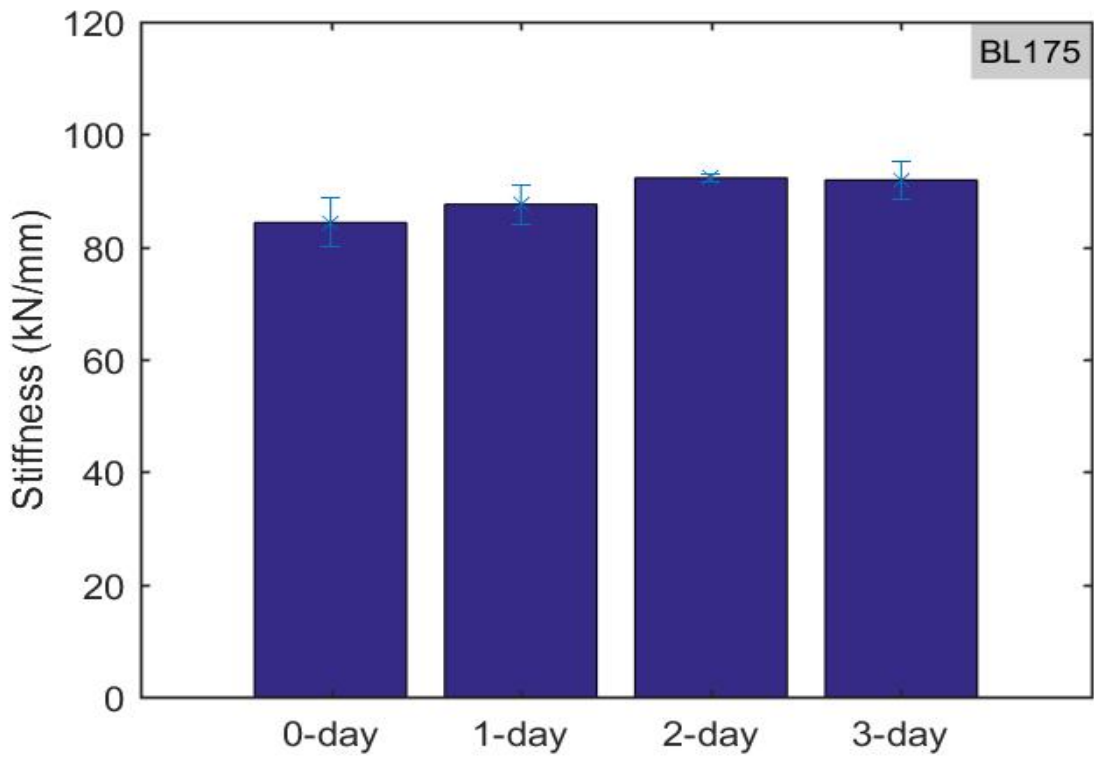


**Figure 36.** Stiffness-exposure time relationship for specimen BL175

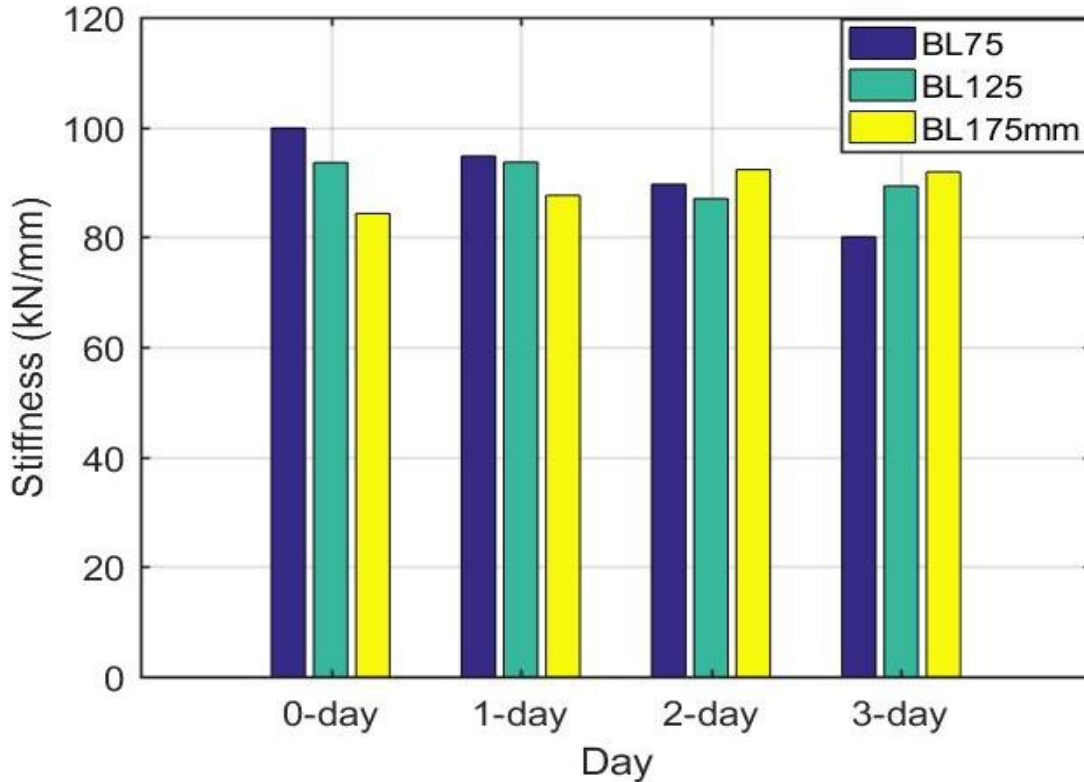


**Figure 37.** Stiffness-exposure time relationship for specimens BL75, BL125 and BL175

#### **4.3.3 Effect of corrosion on joint effective bond length**

The average ultimate loads of joints with different bond lengths are listed in Table 4 and plotted in Figure 38 versus the bond length. It is obvious that the bond strength varied with the bond length. The bond length at which the ultimate load did not significantly change and nearly reached a plateau is defined as effective bond length. For the specimens tested without any exposure to corrosion, the specimens with bond lengths of 75mm, 125 mm, and 175 mm reached average load capacities of 93.50 kN, 98.51 kN, and 100.45 kN, respectively. As the ultimate load capacity increased only a little when the bond length increased from 125 mm to 175 mm, the effective bond length without any exposure can be considered to be 125 mm. Similar conclusions can be made for the specimens experienced 1-day corrosion exposure. However, for the specimens exposed to corrosion for 2 or 3 days, the load capacity kept increasing when the bond length was increased from 125 mm to 175 mm. These results demonstrated that corrosion has a significant

effect on the effective bond length and the effective bond length increased with the exposure duration.

**Table 4** Summary of test results

Test category	Exposure time	Ultimate load capacity (kN)	Average load capacity (kN)
BL75-CS-1	0	96.64	93.50
BL75-CS-2	0	102.5	
BL75-CS-3	0	81.36	
BL75-A-1	24	91.55	89.32
BL75-A-2	24	95.04	
BL75-A-3	24	81.36	
BL75-B-1	48	100.05	80.58
BL75-B-2	48	73.23	
BL75-B-3	48	68.45	
BL75-C-1	72	51.1	66.69
BL75-C-2	72	99.2	
BL75-C-3	72	49.78	
BL125-CS-1	0	102.97	98.51
BL125-CS-2	0	93.74	
BL125-CS-3	0	98.83	
BL125-A-1	24	91.82	93.90
BL125-A-2	24	97.08	
BL125-A-3	24	92.79	
BL125-B-1	48	84.7	81.05
BL125-B-2	48	77.87	
BL125-B-3	48	80.57	
BL125-C-1	72	87.46	78.40
BL125-C-2	72	85.45	
BL125-C-3	72	62.3	
BL175-CS-1	0	109.19	100.45
BL175-CS-2	0	87.4	
BL175-CS-3	0	104.75	
BL175-A-1	24	94.88	96.89
BL175-A-2	24	90.94	
BL175-A-3	24	104.85	
BL175-B-1	48	93.47	88.55
BL175-B-2	48	75.27	
BL175-B-3	48	96.92	
BL175-C-1	72	83.88	83.48
BL175-C-2	72	78.04	
BL175-C-3	72	88.53	

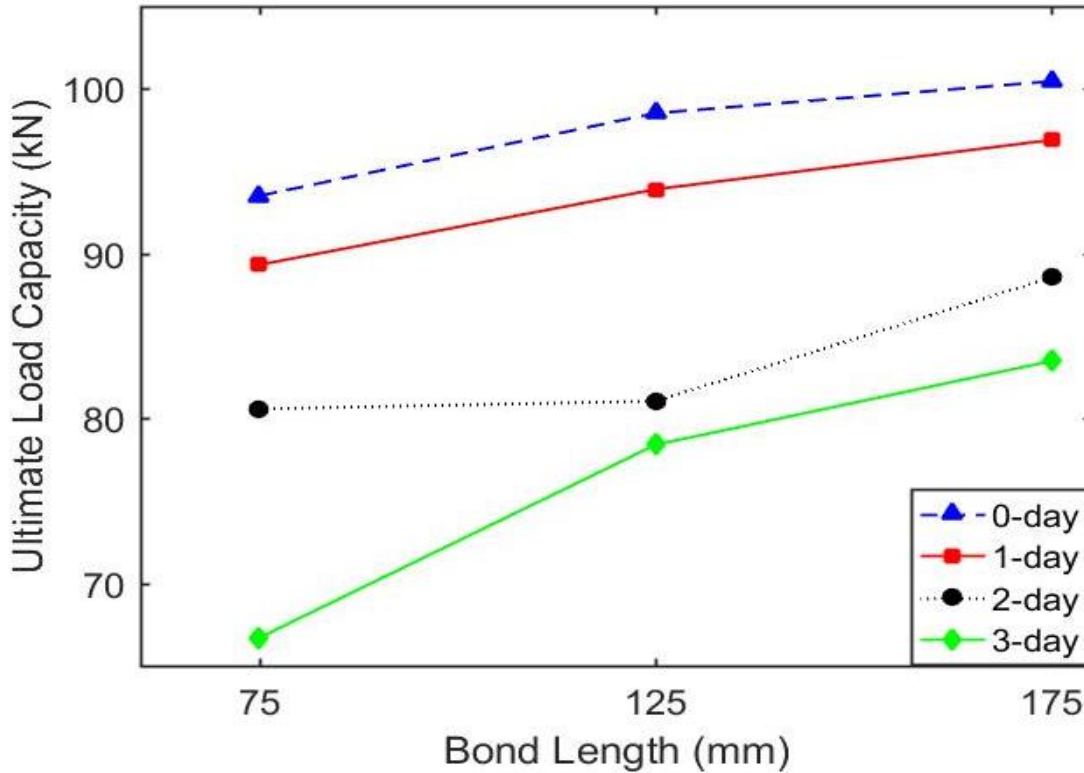


**Figure 38.** Ultimate load capacity versus bond length

#### 4.3.4 Effect of corrosion on joint strength

Bond strengths of the double strap joints, defined as the failure load divided by the bonded area, were calculated for all tested specimens. Figures 39 to 41 shows the bond strength at different exposure durations for the specimens with bond lengths of 75 mm, 125 mm, and 175 mm, respectively. Figure 42 shows the variation of bond strength with both exposure time and bond length. It can be seen that corrosion negatively affected the ultimate strength of all the joints. The decrease in the joint strength were 28.7% for BL75, 20.4% for BL125 and 16.9% for BL175 after the 3-days exposure duration compared to the unconditioned specimens. It should be noted that a larger reduction was observed for the specimens with smaller bond length. For joints with debonding failure mode, the strength showed a considerable reduction. These results suggest that joints with sufficient bond length or with strong adhesive/steel interface experienced insignificant strength reductions. The measured loss of the strength is likely due to the loss of cross-sectional area of the coupons, interfacial attack and/or degradation of the properties of adhesive.

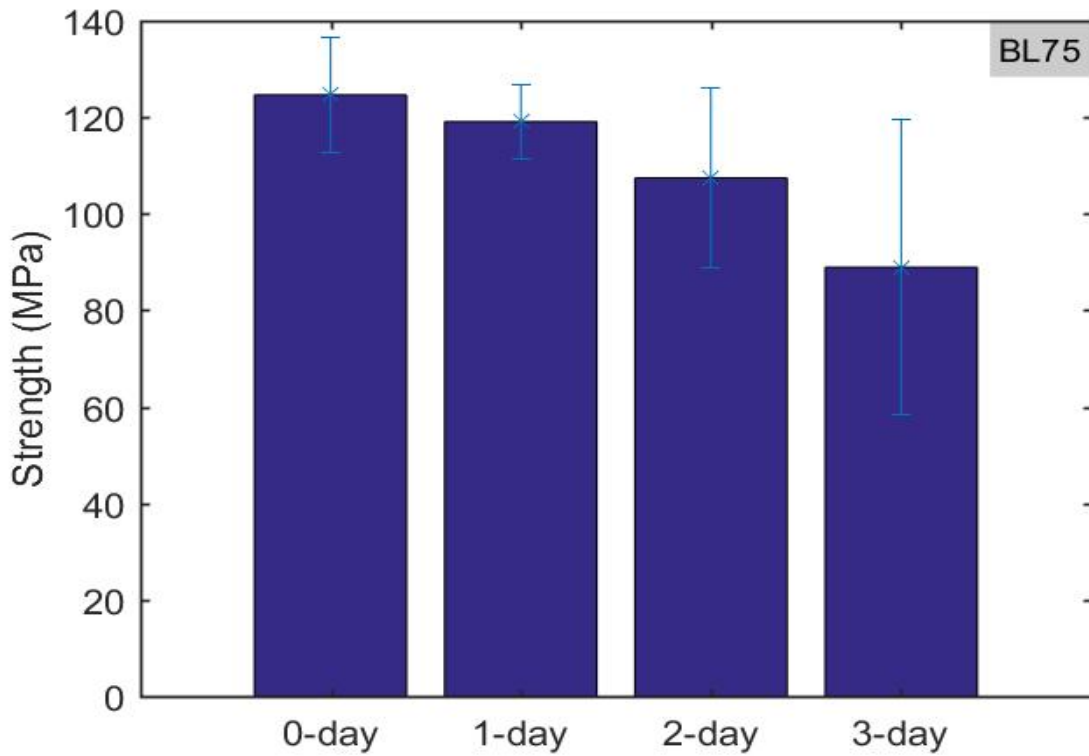


**Figure 39.** Strength-exposure time relationship for specimen BL75

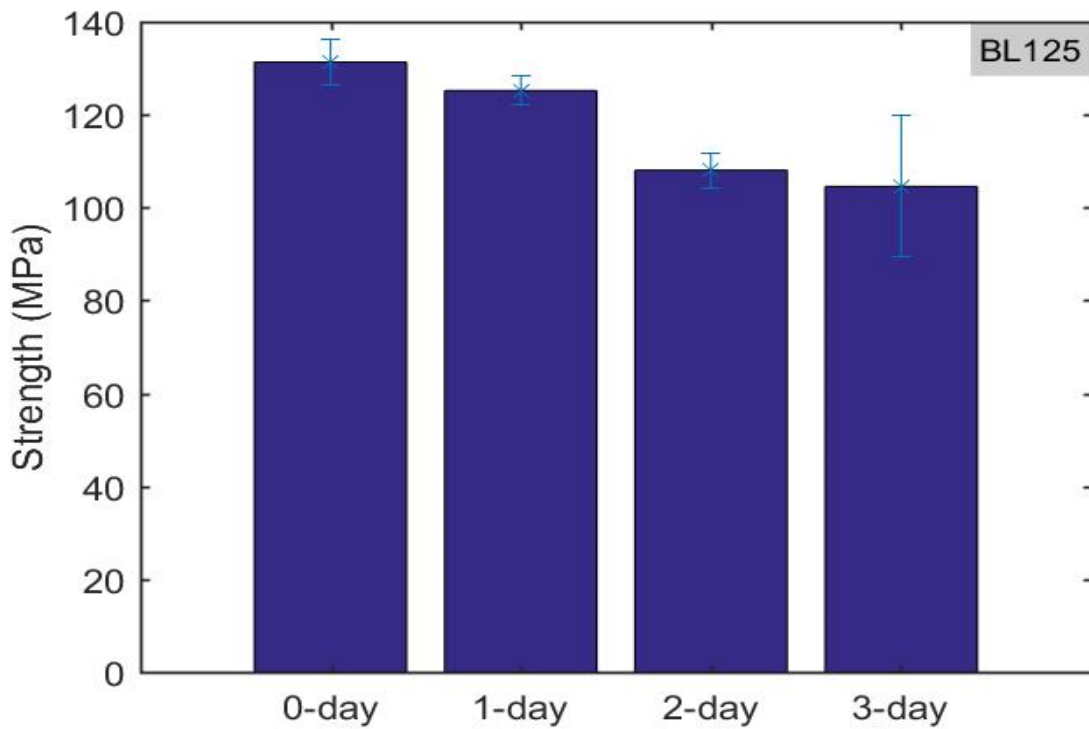


**Figure 40.** Strength-exposure time relationship for specimen BL125

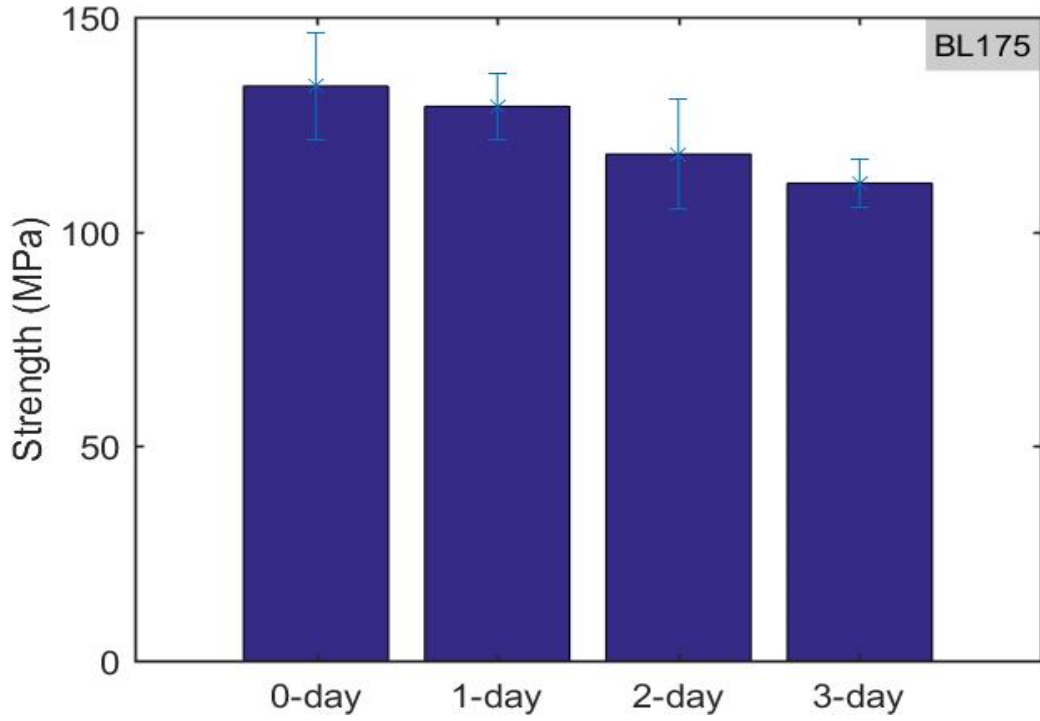


**Figure 41.** Strength-exposure time relationship for specimen BL175

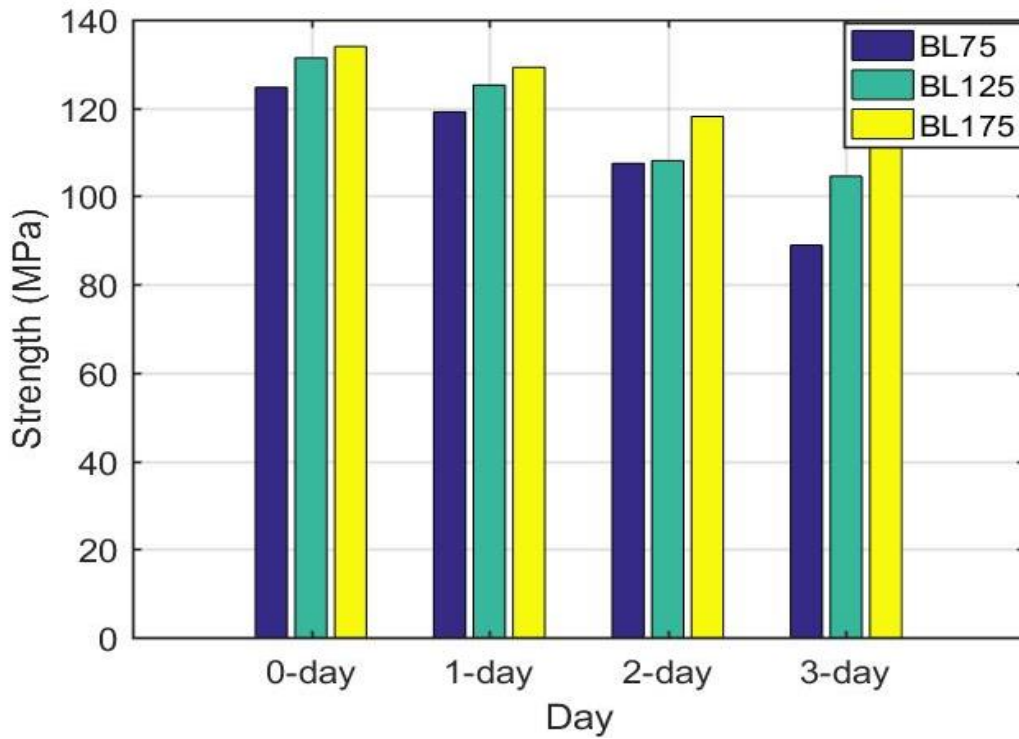


**Figure 42.** Strength-exposure time relationship for specimens BL75, BL125 and BL175

#### **4.3.5 Effect of corrosion on failure modes**

For double strap joint specimens under tensile testing, all specimens failed by the CFRP rupture at the gap as shown in Figure 43, with the exception of specimens BL75-B-3, BL75-C-1 and BL75-C-3. These three specimens failed at load levels of 68.45 kN, 51.1 kN and 49.78 kN due to sudden debonding of CFRP sheets from the steel surface, which proved that the propagation debonding caused the decrease of the ultimate load capacity. This debonding failure was firstly initiated from one end, and then progressed toward the other end followed by the rapid detachment of CFRP from the steel plate, as shown in Figures 44 and 45. The discoloration of debonded region in Figure 45 revealed that moisture may permeated into the interfacial region between the primer and adhesive and therefore caused the degradation of the interface. In addition, experiments on double strap joints with different bond lengths have revealed that the debonding potential decreased with the increased bond length and the debonding failure increased with the exposure duration. However, for the specimen with bond lengths of 125 mm and 175 mm under normal conditions or exposed to the solution for different exposure time, the debonding failure did not occur. This means that when the appropriate bond length was chosen in practice, the debonding failure can greatly be eliminated. For the CFRP rupture failure mode shown in Figure 46, it indicated the full utilization of fibers within the unidirectional sheets. For the specimens with bond lengths of 125 mm and 175 mm, the failure mode was always CFRP rupture independent of the exposure duration, which confirms good bond quality and adhesive/steel stability after immersion in the solution. Similar observations were also indicated by Liu [58]. He concluded that fiber breakage failure was often observed at the joints with high modulus CFRP.

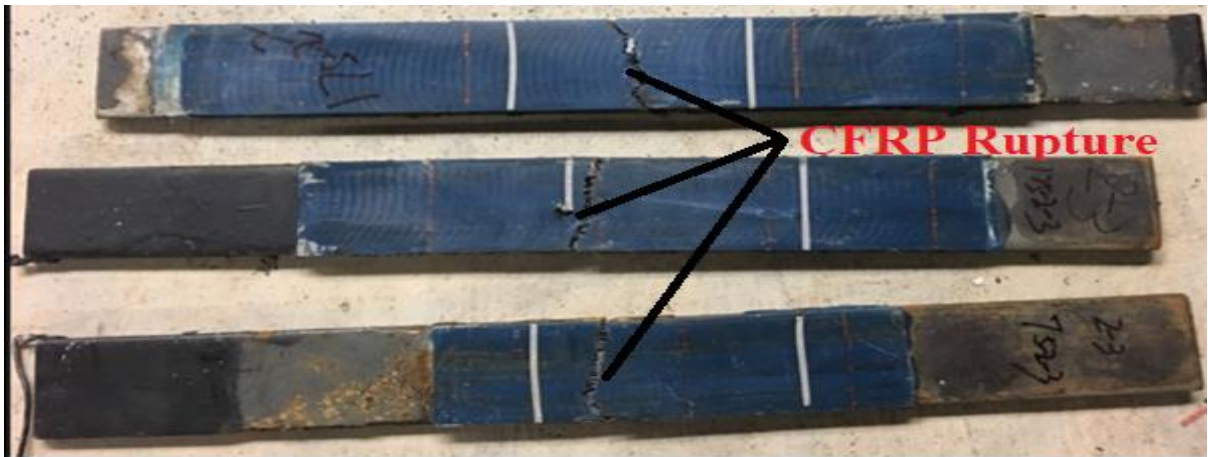


**Figure 43.** CFRP rupture at the gap



**Figure 44.** Debonding failure

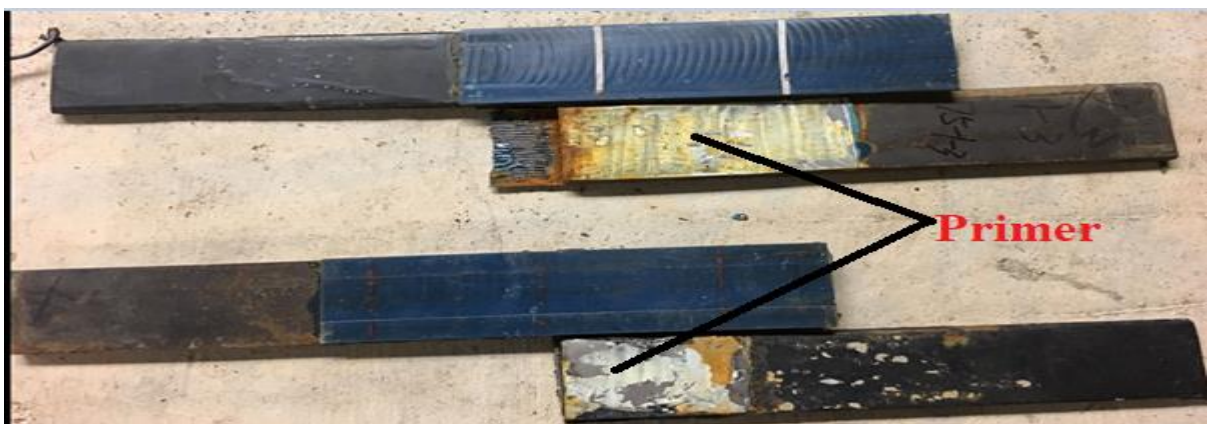


**Figure 45.** Debonding of epoxy from primer

## 5. CONCLUSIONS AND RECOMMENDATIONS

This research aims to study the bond characteristics and behavior of steel plate double strap joints strengthened with CFRP strand sheets considering accelerated corrosion exposures. Since failure of these joints can occur in the interface among different materials, the properties of adhesive, primer and CFRP strand sheets used in double strap joints were studied. In order to obtain the mechanical properties, tensile tests were conducted on epoxy, primer and CFRP strand sheets samples. A total of 36 double strap joint specimens were then fabricated and exposed to the corrosive conditions up to three days. Finally, tensile testing of double strap joints was conducted in a MTS load frame. The effective bond length, failure modes, ultimate capacity of double strap joints and the environmental durability of these joints were evaluated. The research findings led to the following conclusions:

- Most of the tested joints failed due to the rupture of the CFRP strand sheets, which can be avoided by using more layers of CFRP. This indicates that the proposed strengthening system for steel structures using small-diameter CFRP strands can eliminate the debonding failure and ensure satisfactory performance in service. This good bond behavior between CFRP strand sheets and steel plate was achieved due to the entire coverage of the small-diameter strands by the epoxy.
- An effective bond length of 125 mm was identified for CFRP-steel joints under normal conditions. In addition, the effective bond length was found to increase with the exposure time.
- When the double strap joints were exposed to simulated corrosive environments, the joint strength decreased with the increase of exposure time. This may be a consequence of damaging effects of solution on the strength of CFRP. Joints with strong adhesive/steel interface or longer bond length caused the insignificant strength reduction even though the specimens were exposed to the solution for three days.
- For joints with debonding failure mode, the loss of joint strength may be due to the weakening of the adhesive/steel interface. For joints with CFRP rupture failure mode, the degradation of CFRP caused the reduction of joints strength.
- The presence of the primer likely helped to prevent the corrosion of steel plates and increased the durability of the double strap joints under corrosive conditions.

- The stiffness degradation of joints was negligible for all of the bond configurations studied. This characteristic of double strap joints after immersion in the solution for different exposure time revealed negligible changes of properties of adhesive and proved that the adhesive layer is still a strong link under different exposure duration.

While several interesting conclusions regarding the bond behavior of CFRP-steel joints under simulated corrosive environment was drawn, additional research work is needed to confirm the effective application of CFRP strand sheets in strengthening steel structures in practice. Recommended future work is listed as follows:

- Additional experiments need to be conducted with multiple layers of CFRP strand sheets in the joints to study the effect of CFRP layer on the bond characteristics under corrosive environments.
- The degradation of the material properties of adhesive can contribute to the overall joints degradation and the diffusion of water into the adhesive negatively affects the properties of adhesive, so considerable testing on the adhesive should be conducted to evaluate the effects of moisture absorption on the adhesive properties.
- Results obtained from accelerated corrosion tests can be compared with those obtained from specimens experienced long-term exposure to environment.
- The fatigue behavior of the CFRP strand sheet-steel joints can be studied to verify the performance of double strap joints under increased live load levels which are commonly applied to strengthened members.
- The environmental durability of the strengthening system under extended exposure to aggressive environmental conditions (longer durations than those selected in this study) can be evaluated to provide additional information regarding the deterioration mechanism of the strengthening system.
- Effects of other environmental factors such as temperature and humidity on the bond behavior should be investigated in detail to give a comprehensive understanding of the performance of these joints under various environmental conditions.

## REFERENCES

- [1] Lee, S. K. (2012). Current state of bridge deterioration in the U.S. *Materials Performance, NACE International*, 51(2), 2-7.
- [2] Baglin, C. (2014). Response to extreme weather impacts on transportation systems. *Project 20-05 (Topic 44-08)*.
- [3] Mertz, D. R., and Gillespie Jr, J. W. (1996). Rehabilitation of steel bridge girders through the application of advanced composite materials (No. NCHRP-IDEA Project 011).
- [4] Nozaka, K., Shield, C. K., and Hajjar, J. F. (2005). Effective bond length of carbon-fiber-reinforced polymer strips bonded to fatigued steel bridge I-girders. *Journal of Bridge Engineering*, 10(2), 195-205.
- [5] Muthumani, A. and Shi, X. (2015). Impacts of specialized hauling vehicles on highway infrastructure, the economy, and safety: renewed perspective. *International Symposium on Systematic Approaches to Environmental Sustainability in Transportation*.
- [6] Load Rating of Specialized Hauling Vehicles. (2013). <http://www.fhwa.dot.gov/bridge/loadrating/131115.cfm>
- [7] Sivakumar, B. (2015). SHV posting. *AASHTO Subcommittee on Bridges and Structures*, T-18.
- [8] Seica, M. V., & Packer, J. A. (2007). FRP materials for the rehabilitation of tubular steel structures, for underwater applications. *Composite Structures*, 80(3), 440-450.
- [9] Wu, C., Zhao, X., Duan, W. H., & Al-Mahaidi, R. (2012). Bond characteristics between ultra high modulus CFRP laminates and steel. *Thin-Walled Structures*, 51, 147-157.
- [10] Phan, H. B. (2016). The behaviour of CFRP strengthened steel joints (Doctoral dissertation, University of Tasmania).
- [11] Zhao, X. L., & Zhang, L. (2007). State-of-the-art review on FRP strengthened steel structures. *Engineering Structures*, 29(8), 1808-1823.
- [12] Kamruzzaman, M., Jumaat, M. Z., Ramli Sulong, N. H., & Islam, A. B. M. (2014). A review on strengthening steel beams using FRP under fatigue. *The Scientific World Journal*, 2014.
- [13] Shaat, A., Schnerch, D., Fam, A., & Rizkalla, S. (2004, January). Retrofit of steel structures using fiber-reinforced polymers (FRP): State-of-the-art. In Transportation research board (TRB) annual meeting.

- [14] Teng, J. G., Yu, T., & Fernando, D. (2012). Strengthening of steel structures with fiber-reinforced polymer composites. *Journal of Constructional Steel Research*, 78, 131-143.
- [15] Mertz, D. R., & Gillespie Jr, J. W. (1996). Rehabilitation of steel bridge girders through the application of advanced composite materials (No. NCHRP-IDEA Project 011).
- [16] Sen, R., Liby, L., & Mullins, G. (2001). Strengthening steel bridge sections using CFRP laminates. *Composites Part B: Engineering*, 32(4), 309-322.
- [17] Miller, T., Chajes, M., Mertz, D., and Hastings, J. (2001). Strengthening of a Steel Bridge Girder Using CFRP Plates. *J. Bridge Eng.*, 10.1061/(ASCE)1084-0702(2001)6:6(514), 514-522.
- [18] Colombi, P., and Poggi, C. (2006). An experimental, analytical and numerical study of the static behavior of steel beams reinforced by pultruded CFRP strips. *Composites Part B: Engineering*, 37(1), 64-73.
- [19] Schnerch, D., and Rizkalla, S. (2008). Flexural strengthening of steel bridges with high modulus CFRP strips. *Journal of Bridge Engineering*, 13(2), 192-201.
- [20] Rizkalla, S., Dawood, M., and Schnerch, D. (2008). Development of a carbon fiber reinforced polymer system for strengthening steel structures. *Composites Part A: Applied Science and Manufacturing*, 39(2), 388-397.
- [21] Dawood, M., and Rizkalla, S. (2010). Environmental durability of a CFRP system for strengthening steel structures. *Construction and Building Materials*, 24(9), 1682-1689.
- [22] Schnerch, D., Dawood, M., Rizkalla, S., and Sumner, E. (2007). Proposed design guidelines for strengthening of steel bridges with FRP materials. *Construction and building materials*, 21(5), 1001-1010.
- [23] Fam, A., MacDougall, C., and Shaat, A. (2009). Upgrading steel–concrete composite girders and repair of damaged steel beams using bonded CFRP laminates. *Thin-Walled Structures*, 47(10), 1122-1135.
- [24] Al-Saidy, A. H., Klaiber, F. W., and Wipf, T. J. (2007). Strengthening of steel–concrete composite girders using carbon fiber reinforced polymer plates. *Construction and Building Materials*, 21(2), 295-302.
- [25] Narmashiri, K., Jumaat, M. Z., and Sulong, N. R. (2010). Shear strengthening of steel I-beams by using CFRP strips. *Scientific Research and Essays*, 5(16), 2155-2168.

- [26] Patnaik, A. K., Bauer, C. L., and Srivatsan, T. S. (2008). The extrinsic influence of carbon fibre reinforced plastic laminates to strengthen steel structures. *Sadhana*, 33(3), 261-272.
- [27] Jiao, H., Phan, H., and Zhao, X. (2014). Fatigue Behaviour of Steel Elements Strengthened with Stand CFRP Sheets. *Advances in Structural Engineering*, 17(12), 1719-1728.
- [28] Tabrizi, S., Kazem, H., Rizkalla, S., and Kobayashi, A. (2015). New small-diameter CFRP material for flexural strengthening of steel bridge girders. *Construction and Building Materials*, 95, 748-756.
- [29] Kazem, H., Guaderrama, L., Selim, H., Rizkalla, S., and Kobayashi, A. (2016). Strengthening of steel plates subjected to uniaxial compression using small-diameter CFRP strands. *Construction and Building Materials*, 111, 223-235.
- [30] Teng, J. G., Fernando, D., Yu, T., & Zhao, X. L. (2012, February). Debonding failures in CFRP-strengthened steel structures. In Proceedings of the Third Asia-Pacific Conference on FRP in Structures. Japan: Hokkaido University.
- [31] Fawzia, S., Al-Mahaidi, R., Zhao, X. L., & Rizkalla, S. (2007). Strengthening of circular hollow steel tubular sections using high modulus CFRP sheets. *Construction and Building Materials*, 21(4), 839-845.
- [32] Al-Zubaidy, H. A., Zhao, X. L., & Al-Mahaidi, R. (2013). Experimental evaluation of the dynamic bond strength between CFRP sheets and steel under direct tensile loads. *International Journal of Adhesion and Adhesives*, 40, 89-102
- [33] Liu, M., & Dawood, M. (2017). Reliability analysis of adhesively bonded CFRP-to-steel double lap shear joint with thin outer adherends. *Construction and Building Materials*, 141, 52-63.
- [34] Batuwitage, C., Fawzia, S., Thambiratnam, D., & Al-Mahaidi, R. (2017). Durability of CFRP strengthened steel plate double-strap joints in accelerated corrosion environments. *Composite Structures*, 160, 1287-1298.
- [35] Taylor, C., Jiao, H., Zhao, X. L., & Kobayashi, A. (2013). Debonding strength of steel joints strengthened using strand CFRP sheets under axial tension. In Fourth Asia-Pacific Conference on FRP in Structures (APFIS 2013) (pp. 1-6).
- [36] Linghoff, D., Al-Emrani, M., & Kliger, R. (2010). Performance of steel beams strengthened with CFRP laminate–Part 1: Laboratory tests. *Composites Part B: Engineering*, 41(7), 509-515.

- [37] Al-Shawaf, A., Al-Mahaidi, R., & Zhao, X. L. (2006, December). Study on bond characteristics of CFRP/steel double-lap shear joints at subzero temperature exposure. In Proc., 3rd Int. Conf. on FRP Composites in Civil.
- [38] Heshmati, M., Haghani, R., & Al-Emrani, M. (2017). Durability of CFRP/steel joints under cyclic wet-dry and freeze-thaw conditions. *Composites Part B: Engineering*, 126, 211-226.
- [39] Nguyen, T. C., Bai, Y., Zhao, X. L., & Al-Mahaidi, R. (2012). Durability of steel/CFRP double strap joints exposed to sea water, cyclic temperature and humidity. *Composite Structures*, 94(5), 1834-1845.
- [40] Nguyen, T. C., Bai, Y., Zhao, X. L., & Al-Mahaidi, R. (2011). Mechanical characterization of steel/CFRP double strap joints at elevated temperatures. *Composite Structures*, 93(6), 1604-1612.
- [41] Nguyen, T. C., Bai, Y., Al-Mahaidi, R., & Zhao, X. L. (2012). Time-dependent behaviour of steel/CFRP double strap joints subjected to combined thermal and mechanical loading. *Composite Structures*, 94(5), 1826-1833.
- [42] Nguyen, T. C., Bai, Y., Zhao, X. L., & Al-Mahaidi, R. (2012). Effects of ultraviolet radiation and associated elevated temperature on mechanical performance of steel/CFRP double strap joints. *Composite Structures*, 94(12), 3563-3573.
- [43] Heshmati, M. (2015). Hygrothermal durability of adhesively bonded FRP/steel joints.
- [44] Agarwal, A., Foster, S. J., & Hamed, E. (2016). Testing of new adhesive and CFRP laminate for steel-CFRP joints under sustained loading and temperature cycles. *Composites Part B: Engineering*, 99, 235-247.
- [45] Sahin, M. U., & Dawood, M. (2016). Experimental investigation of bond between high-modulus CFRP and steel at moderately elevated temperatures. *Journal of Composites for Construction*, 20(6), 04016049.
- [46] Borrie, D., Liu, H. B., Zhao, X. L., Raman, R. S., & Bai, Y. (2015). Bond durability of fatigued CFRP-steel double-lap joints pre-exposed to marine environment. *Composite Structures*, 131, 799-809.
- [47] Heshmati, M., Haghani, R., & Al-Emrani, M. (2017). Durability of bonded FRP-to-steel joints: Effects of moisture, de-icing salt solution, temperature and FRP type. *Composites Part B: Engineering*, 119, 153-167.

- [48] Bai, Y., Nguyen, T. C., Zhao, X. L., & Al-Mahaidi, R. (2013). Environment-assisted degradation of the bond between steel and carbon-fiber-reinforced polymer. *Journal of Materials in Civil Engineering*, 26(9), 04014054.
- [49] Nguyen, T. C., Bai, Y., Zhao, X. L., & Al-Mahaidi, R. (2013). Curing effects on steel/CFRP double strap joints under combined mechanical load, temperature and humidity. *Construction and Building Materials*, 40, 899-907.
- [50] Batuwitige, C., Fawzia, S., Thambiratnam, D., & Al-Mahaidi, R. (2017). Evaluation of bond properties of degraded CFRP-strengthened double strap joints. *Composite Structures*, 173, 144-155.
- [51] Kabir, M. H., Fawzia, S., Chan, T. H., & Badawi, M. (2016). Durability of CFRP strengthened steel circular hollow section member exposed to sea water. *Construction and Building Materials*, 118, 216-225.
- [52] Kim, Y. J. (2017). Performance of steel girders repaired with advanced composite sheets in a corrosive environment (No. MPC 17-325). Mountain Plains Consortium.
- [53] Hidekuma, Y., Kobayashi, A., Okuyama, Y., Miyashita, T., & Nagai, M. (2012). Experimental study on debonding behavior of CFRP for axial tensile reinforced steel plate by CFRP strand sheets. In *The Third Asia-Pacific Conference on FRP in Structures (APFIS2012)*, Hokkaido University, Japan.
- [54] Ahmad, Z. (2006). Principles of corrosion engineering and corrosion control. *Elsevier*.
- [55] Standard, A. S. T. M. (2004). G102-89. Calculation of corrosion rates and related information from electrochemical measurements, Annual Book of ASTM Standards, ASTM International, Philadelphia.
- [56] Standard, A. S. T. M. (2010). D638-10, 2010. Standard test method for tensile properties of plastics,” ASTM International, West Conshohocken, PA.
- [57] Standard, A. S. T. M. (2008). Standard test method for tensile properties of polymer matrix composite materials. ASTM D3039/D M, 3039, 2008.
- [58] Deng, J., & Lee, M. M. (2007). Behaviour under static loading of metallic beams reinforced with a bonded CFRP plate. *Composite Structures*, 78(2), 232-242.
- [59] ISO 4624: Paint and varnishes — pull-off test, ISO, Geneva, Switzerland, 1978.

- [60] El Maaddawy, T. A., & Soudki, K. A. (2003). Effectiveness of impressed current technique to simulate corrosion of steel reinforcement in concrete. *Journal of materials in civil engineering*, 15(1), 41-47.
- [61] Standard, A. S. T. M. (2003). G1-03. Standard Practice for preparing, cleaning, and evaluating corrosion test specimens, *Annual Book of ASTM Standards*, 3, 17-25.
- [62] Tamura, H. (2008). The role of rusts in corrosion and corrosion protection of iron and steel. *Corrosion Science*, 50(7), 1872-1883.